

Research paper

Performance improvement of flat plate solar collector employing phase change material bags and hybrid nanofluid



Mohammed Alktranee^a, Qudama Al-Yasiri^b, Mushtaq A. Al-Furaiji^b,
Hassan A. Hameed Al-Hamzawi^c, Péter Bencs^{d,*}, Márta Szabó^e

^a Department of Mechanical Techniques, Technical Institute of Basra, Southern Technical University, Basrah, Iraq

^b Department of Petroleum Engineering, College of Engineering, University of Misan, Al Amarah city, 62001, Iraq

^c Ministry of Construction, Housing, Municipalities and Public Works, Diwaniyah, Iraq

^d Department of Fluid and Heat Engineering, Faculty of Mechanical Engineering and Informatics, University of Miskolc, Miskolc, HU-3515, Hungary

^e Department of Building Engineering and Energetics, Institute of Technology, MATE, Szent István Campus, Páter K. U. 1, Gödöllő, H-2100, Hungary

ARTICLE INFO

ABSTRACT

Keywords:

Solar collector
Water heating
PCM
Hybrid nanofluid
Energy gain
Exergy analysis

The current paper explores the dual influence of phase change material (PCM) and hybrid nanofluid to improve and prolong the productivity of a traditional flat plate solar collector (FPSC). Experimentally, two identical FPSCs were designed, fabricated and examined under hot weather conditions, considering numerous thermal, energy, exergy and economic aspects. PCM-microencapsulated thermal bags and Multiwall Carbon Nanotube-Aluminum Oxide (MWCNT- Al₂O₃) nanofluid with 0.15 % and 0.2 % concentrations were investigated in three different cases compared to a reference case. The PCM bags were integrated behind the FPSC absorber in one case, while the other cases explored the improvement of circulating MWCNT-Al₂O₃ nanofluid with 0.15 % and 0.2 % concentrations. Study findings indicated that the FPSC output temperature was improved by employing PCM bags and enhanced further when introducing MWCNT-Al₂O₃ hybrid nanofluid. Specifically, energy analysis displayed that the energy gain improvement reached up to 26 %, 47 % and 54 %, for the FPSC integrating PCM, PCM with MWCNT- Al₂O₃ nanofluid at 0.15 % and 0.2 % concentrations, respectively. Moreover, the thermal efficiency for the FPSC integrated PCM, PCM with MWCNT- Al₂O₃ at 0.15 % and 0.2 % concentrations, was enhanced by 10 %, 21 % and 26 % over the reference case, while the exergy efficiency was augmented by 9 %, 31 %, and 38 %, respectively. Furthermore, economic analysis displayed that employing PCM with MWCNT-Al₂O₃ hybrid nanofluids at 0.2 % concentration has shortened the FPSC payback period by 25%, verifying the feasibility of the suggested enhancement techniques.

1. Introduction

Solar energy has been recommended as a viable thermal and electrical alternative energy source worldwide, especially for locations with abundant solar radiation [1–3]. Among solar systems, the implementation of solar thermal collectors is witnessing a significant surge as they offer sustainable alternatives to conventional fuel heaters, particularly for low-temperature sanitary applications ranging from 40°C to 80°C [4, 5]. The pursuit of enhanced efficiency in flat plate solar collectors (FPSCs) has spurred innovative research across various methodologies. Recent advancements proposed significant potential for integrating nanofluids, porous media, twisted tapes, fins, baffles, thermal coating,

inserts, turbulators, and reflectors [6–12].

Nanotechnology has presented notable advancements in different research fields, including renewable and non-renewable energy systems [13], water treatment [14], construction [15], electrochemical systems [16], medical aspects [17], power generation [18] and various industrial sectors [19,20]. In the solar energy path, nanotechnology has revolutionised solar systems by enhancing heat transfer abilities and overall efficiency through the integration of nanoparticles into base fluids [21]. Lately, phase change materials (PCMs) have been approved as a successful thermal energy storage approach to be involved in different energy sectors, thanks to their ability to store, release and manage heat noticeably, advancing solar systems notably [22]. Both nanofluids and PCMs have recently been explored as a revolutionary pair to advance

* Corresponding author.

E-mail addresses: mohammed.hr@stu.edu.iq (M. Alktranee), qudamaalyasiri@uomisan.edu.iq (Q. Al-Yasiri), eng.mushtaq@uomisan.edu.iq (M.A. Al-Furaiji), hassanafak@gmail.com (H.A.H. Al-Hamzawi), peter.bencs@uni-miskolc.hu (P. Bencs), szabo.marta@uni-mate.hu (M. Szabó).

| Nomenclature | |
|-----------------------|--------------------------------------|
| <i>Abbreviations</i> | |
| DI | Deionized |
| FPSC | Flat plate solar collector |
| HNF | Hybrid nanofluid |
| <i>Nu</i> | Nusselt number |
| PCM | Phase change material |
| TEM | Transmission Electron Microscopy |
| <i>Re</i> | Reynolds number |
| XRD | X-ray diffraction |
| <i>Symbols</i> | |
| <i>Ac</i> | Collector area |
| <i>b_f</i> | Base fluid |
| <i>C_p</i> | Specific heat |
| <i>h</i> | Convective heat transfer coefficient |
| <i>H</i> | Heat exchanger tube's height |
| <i>l</i> | Heat exchanger tube's length |
| <i>L</i> | Heat exchanger riser length |
| <i>m_{nm}</i> | Mass of the nanomaterials |
| <i>m_{bf}</i> | The mass of the base fluid |
| <i>m̄</i> | Mass flow rate |
| <i>n</i> | Number of tubes |
| <i>n_f</i> | Nanofluid |
| <i>n_m</i> | Nanomaterial |
| <i>k</i> | Thermal conductivity |
| <i>S</i> | Solar radiation |
| <i>W</i> | Tube's width |
| <i>Greek symbols</i> | |
| φ | Volume fraction |
| ρ | base fluid density |
| ρ_{nm} | Nanomaterial density |
| μ | Viscosity |

thermal energy systems [23]. In this regard, Fig. 1 displays the booming progress of research in thermal systems integrated nanofluids and PCM in recent years.

Numerous studies have collectively highlighted significant advancements in the performance of FPSCs using nanofluids and PCMs, offering promising solutions to enhance thermal efficiency and sustainability in solar systems. In a study conducted by Alawi et al. [24], machine-learning models were used to predict the thermal efficiency of FPSCs using Al_2O_3 -water nanofluids. Among the tested models, the Stacking Regressor achieved the highest prediction accuracy at 94.5 %. Key parameters influencing efficiency were identified, showing the strongest correlation with the absorbed heat parameter. These findings have enhanced predictive modelling in thermal engineering, providing valuable insights for optimising FPSC performance. Additionally, the impact of PCM on the FPSC performance was investigated using a novel

binary hydrated salt, in which the thermal conductivity and storage capacity of the system were significantly improved. This method has increased the latent heat by 26.98 J/g and achieved a phase transition temperature of 61.71°C. Recent numerical analysis conducted by Fu et al. [25] revealed substantial improvements in heat transfer and reduced fluid resistance in a novel FPSC design featuring porous media and a chamfered cavity structure. This innovative configuration has achieved an efficiency increase of up to 49.57 %, effectively balancing enhanced performance with minimal pumping power, marking a significant advancement in FPSC technology. Prabhu et al. [26] showed that the thermal performance of the FPSC was highly improved by incorporating porous media. The modified design, including concentric semi-circular riser tubes and PCM, achieved a maximum water temperature of 63.5°C. This integration significantly improved the heat transfer and reduced heat loss by 9.8 %-12.6 %. With energy and exergy

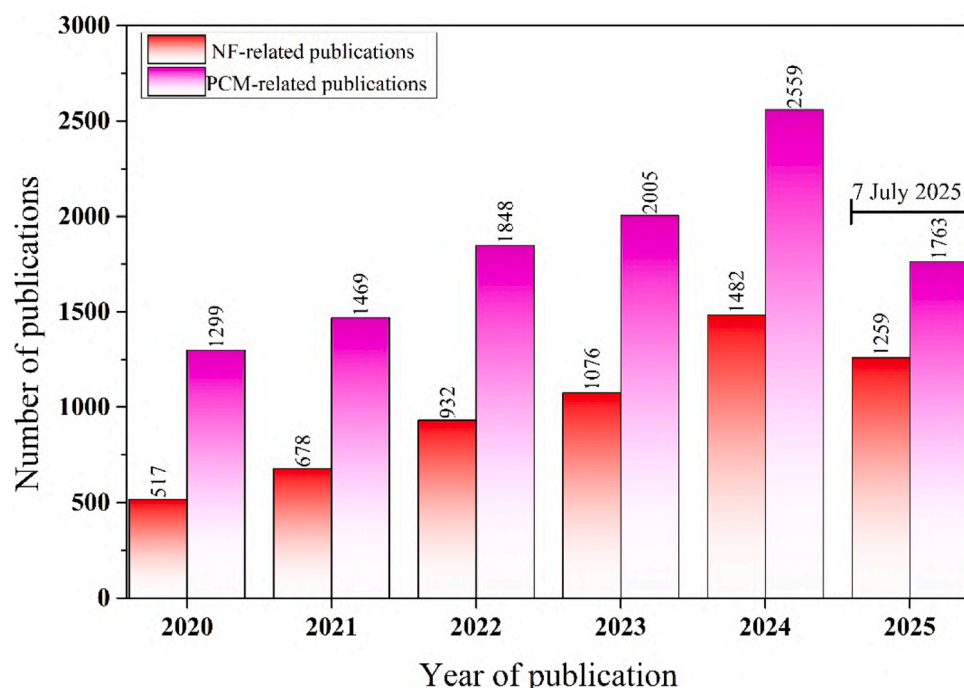


Fig. 1. Number of publications conducted on the use of nanofluids and PCMs to enhance thermal systems according to the Scopus database (Accessed on the 7th of July 2025).

efficiencies of 74 % and 6 %, the system has lowered energy costs by 22.2 % and CO₂ emissions by 58 %, making it a sustainable option for industrial heating applications. Xia et al. [27] have improved the thermal performance of the FPSC by integrating porous metal blocks inside the absorber's inner wall. Various parameters were analysed, including block shape (rectangular, trapezoidal, triangular), permeability, material type (stainless steel, alumina, aluminium, copper), and the number of blocks. Among these, rectangular blocks with high permeability ($\sim 10^{-2}$) and higher Reynolds numbers (Re= 468) showed the greatest improvement in FPSC's heat transfer. Copper blocks provided the best performance, achieving a Nusselt number of 7.17 and enhanced the FPSC efficiency by 80 %. Although this technique has increased the friction factor due to pressure drops, the performance evaluation criteria indicated that the efficiency gains outweighed the resistance. Sathish et al. [28] investigated the thermal performance of the FPSC using various nanomaterials (including Al₂O₃, Cu, MWCNT, and SiO₂) and their hybrid combination. Outcomes revealed that the hybrid nanofluids (HNFs), composed of 25 % each of Al₂O₃, Cu, MWCNT, and SiO₂, have significantly enhanced heat transfer, thermal conductivity, and overall efficiency. The FPSC achieved peak outlet temperatures of 83.2°C, a heat gain of 2385 W, and a thermal efficiency of 70.4 %. These results underscored the substantial advantages of HNFs over monodisperse fluids in FPSCs, suggesting that future work should focus on optimizing particle sizes and fluid flow for further performance enhancement. Akram et al. [29] explored the application of PEG-Fe₃O₄ nanofluid in the FPSC using a novel in-situ oxidation precipitation technique. Characterization methods such as FESEM, XRD, and FTIR confirmed successful covalent functionalization, leading to a 13.35 % increase in thermal conductivity, along with improvements in density, specific heat, and viscosity. Experimental tests demonstrated the FPSC thermal efficiency improvement of 13.83 % under specific conditions, with numerical analysis via ANSYS CFD matching experimental data with a deviation of 8.33 %. This research has highlighted the potential of PEG-Fe₃O₄ nanofluid in enhancing solar energy systems for sustainable heat transfer. Alfellag et al. [30] explored the thermal and exergy efficiency of FPSCs using eco-friendly clove-treated CT-MWCNTs/TiO₂ HNFs dispersed in distilled water. Testing different weight concentrations (from 0.025 % to 0.1 %) and flow rates from 0.3 to 1.2 L/min showed a 20.6 % increase in thermal efficiency and a 22.9 % rise in exergy efficiency. Consequently, the collector size was reduced by 20.5 %, and HNFs outperformed mono nanofluids. In a recent study conducted by Suqi et al. [31] to investigate the FPSC performance of using an external magnetic field, water-Fe₃O₄ ferrofluid, and twisted tape turbulators. The study analyzed various key parameters such as the outlet temperature, pressure drop, thermal energy transfer, and entropy generation rates across varying tube cross-sections and Reynolds numbers. The findings indicated that circular tubes outperform triangular ones in terms of thermal efficiency. The application of nano-enhanced PCM to improve the FPSC was studied by Bharathiraja et al. [32], combining paraffin wax with MWCNT and SiO₂ at 1 wt %. study outcomes showed that the FPSC output water temperature was elevated by 67°C to 70°C, and the collector thermal efficiency enhanced using nano-enhanced PCM by 5 %- 7 % over the reference FPSC. The same approach was followed by Sharma et al. [33] employing three different combinations. As a general observation, the study found that the nano-enhanced PCMs have significantly increased the heat charging and discharging, augmenting the overall heat gain to up to 12 %, over the reference case.

The study aims to comparatively investigate the combined role of integrating PCM and HNF into FPSCs to enhance its techno-economic performance, seeking to address the limitations of conventional systems. Unlike other literature studies, the current work proposed the PCM and HNF to work individually to improve the FPSC performance, avoiding complex integration and stability issues of nano-enhanced PCM. The FPSC thermal performance is investigated and analysed considering the temperature distribution and elevation of the output water temperature. Energetically, the energy gain, thermal efficiency,

FPSC exergy and sustainability index have been evaluated and quantified. Eventually, a comprehensive economic analysis was presented to assess the cost-effectiveness of integrating PCM bags and HNF into the FPSC, highlighting their role in minimising the payback period. By accomplishing these aims, this work will contribute to the advancement of solar energy technology and provide valuable insights for the design and implementation of more efficient and sustainable solar heating systems.

2. Methodology

2.1. FPSC configuration and measurements

The FPSC was locally designed with internal dimensions of 100 cm length, 50 cm width and 20 cm height. The collector consisted mainly of a 2 mm thick galvanised plate painted with black colour for maximum absorptivity, and copper pipes (9 mm diameter) attached directly above the absorbing plate. Positioning the serpentine pipes above the absorber plate, rather than attached to the rear side or embedded within it, is a fundamental configuration adopted to augment the heat transfer efficiency of FPSC by allowing for better contact between the fluid and the heated absorbing plate [34]. The absorbing plate was enclosed with wool thermal insulation and wooden blocks on each side, then the backside of the FPSC was shielded by a wooden plate. Besides, the top of the FPSC was enclosed by a glass sheet with a 2 mm thickness. The FPSC has delivered various working fluids utilising a pump placed in a plastic container and connected with a flow rate sensor set at 1.8 kg/min. A temperature sensor was installed in the entrance port of the FPSC to measure the temperature variance. Furthermore, the outlet fluid was also measured using another temperature sensor placed at the outlet port and then circulated into a copper coil placed in a well-insulated plastic water tank of 55 litres. All plastic tanks, containers, copper coil surfaces, and PCM bags were provided with temperature sensors. The real experimental setup and schematic diagram of the developed FPSCs are indicated in Fig. 2, showing all parts and places of the temperature sensors.

Temperature profiles during experiments were measured and documented using ATmega 2560 data logger every 10 min from 7:00 to 18:00. Besides, the solar radiation variation during the sunshine period was measured using a handheld solar power meter, while wind speed throughout the experiment period was recorded using an anemometer. A thermal imaging camera was used to visualise the temperature behaviour of the reference and improved FPSC. Table 1 demonstrates the specifications of the instruments used for measurements.

The experiments were performed using 10 PCM bags holding 150 g each, placed at the backside of the modified FPSC (Fig. 3). Therefore, three temperature sensors were immersed in three different positions of three PCM bags to track the temperature behaviour of PCM during the melting and solidification phases. To further improve FPSC performance, the experiments were performed using hybrid MWCNT-Al₂O₃ nanofluids circulated into the serpentine pipe at different volume fractions (namely, 0.15 % and 0.2 %).

2.2. Preparation of PCM bags

The current study mainly examines the effect of using PCM on the thermal performance of FPSC under the effect of water and HNF. The used PCM is an Iraqi paraffin, which is produced as a waste wax in the Iraqi petroleum refineries. This wax is yellowish and has good characteristics, such as high heat storage capacity and high melting temperature, appropriate for many applications. Table 2 shows the thermophysical features of paraffin wax [35]. The PCM was scaled with 150 g and melted by an electric boiler (size 0.75 L) and poured into thermal bags (roasting bags with temperature resistance by up to 200 °C) with 9 × 14 × 1.3 cm dimensions, collecting a total of 10 bags (i.e., 1500 g). Afterwards, PCM bags were left to solidify and placed between

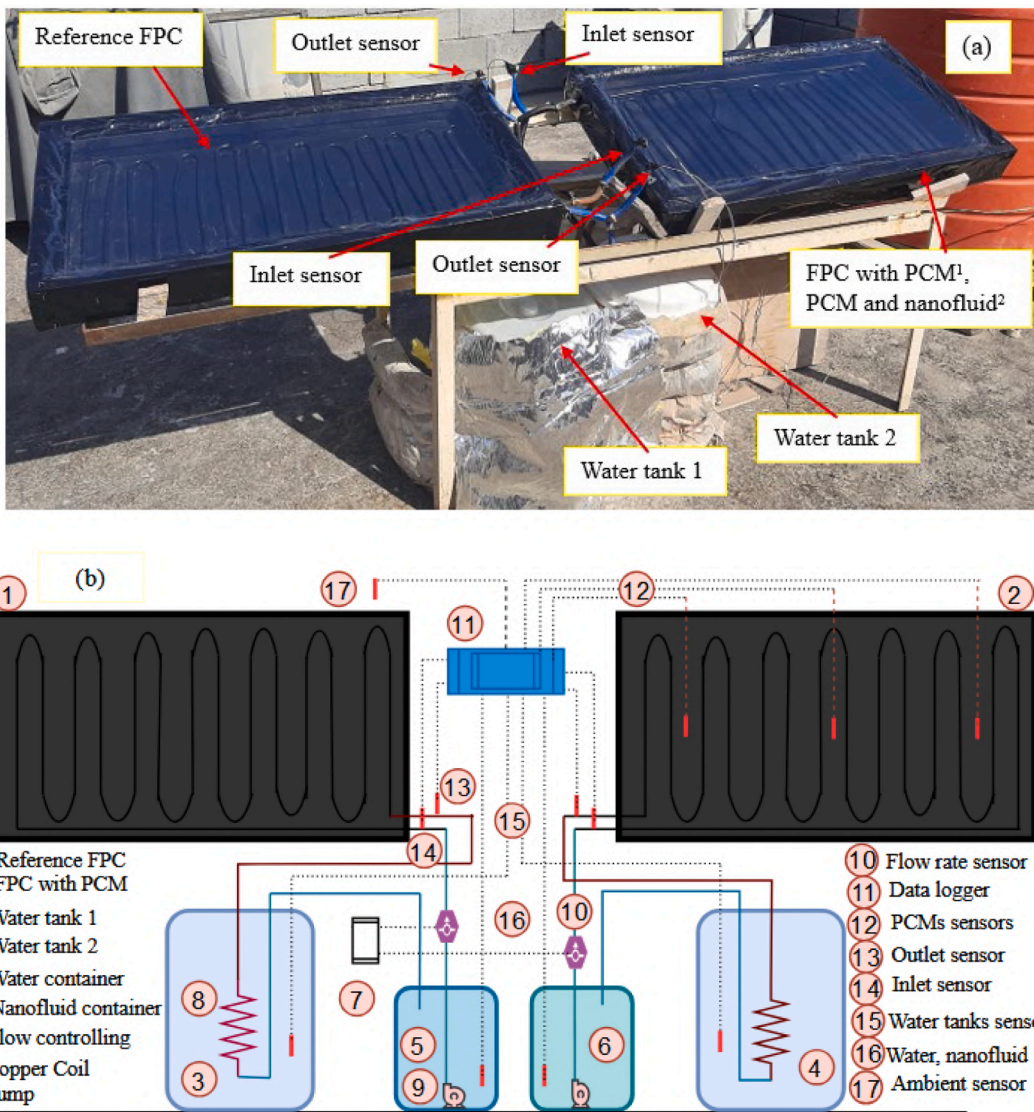


Fig. 2. Experimental setup (a) view of FPSCs and accessories, (b) schematic diagram of the system and measurement sensors.

the backside of the modified FPSC and thermal insulation, incorporating three temperature sensors as stated earlier. Fig. 3 displays the preparation procedure for PCM bags.

2.3. Preparation of hybrid nanomaterials

The hybrid nanomaterials employed in the current work comprised Multi-walled Carbon nanotubes (MWCNTs) and Aluminium Oxide (Al_2O_3) nanoparticles, which were prepared as the MWCNTs/ Al_2O_3 composite with 50 %:50 %. The hybrid MWCNT- Al_2O_3 nanomaterials were bought from Nano Research Materials Inc. (USA), and their thermophysical properties were measured in the Department of Polymers, University of Miskolc, Hungary. The surface morphology of MWCNT- Al_2O_3 nanomaterials has been investigated using transmission electron microscopy (TEM), as shown in Fig. 4. The MWCNT- Al_2O_3 nanomaterials with a diameter ranging between 25–70 nm were measured by HR-TEM images considering the original scale bar. The homogeneously dispersed Al_2O_3 nanoparticles on the MWCNT nanotube could be observed at different micron lengths with diameter ranges (5–12 nm).

2.4. Preparation of nanofluids and measurement of their thermophysical properties

The preparation of stable nanofluids depends on numerous factors, including the type of preparation method (first or second step method), dispersion of nanomaterials into the host fluid, thermophysical properties of nanomaterials, host fluids, sonication period, volume fractions, and many others [36]. Therefore, the hybrid MWCNT- Al_2O_3 nanofluid conducted in this work was prepared adopting the second step method by mixing the hybrid nanomaterials with deionised (DI) water at two volume concentrations: 0.15 % and 0.2 %, employing Eq. (1) [37]. A specific amount of hybrid MWCNT- Al_2O_3 was weighted by a precise electronic scale, dispersed into DI water and mixed by a magnetic stirrer for 25 min. The mixed hybrid nanofluid was placed into a sonication path for 40 min to obtain a homogeneous mixture, fragment the large clusters of hybrid nanomaterials, and achieve stable nanofluids. Fig. 5 illustrates the preparation steps of hybrid nanofluids.

The stability of prepared nanofluids was inspected after the sonication period ended by visualisation and sedimentation methods, taking a sample of nanofluids and leaving it to settle for 2 days. Depending on the time sediment of the hybrid MWCNT- Al_2O_3 nanomaterials into DI water, the nanofluids achieved good stability as seen in the last step of Fig. 5. It is worth noting that the prepared nanofluids were directly used

Table 1

Specifications of instruments according to the manufacturer's datasheet.

| Instrument characteristics | Photo of instrument/tool |
|---|---|
| Thermocouples Model: K-type (2 m length) Measurement range: -200 °C to 1350 °C Accuracy: 0.25 °C |  |
| Solar power meter Model: SM206 Measurement range: 1–3999 W/m ² Accuracy: ± 10 W/m ² |  |
| Water pump Model: Water pump Measurement range: 800 L/h |  |
| Flow rate sensor Model: YF-S201 Measurement range: -25 °C to +80 °C Accuracy: ± 10 % |  |
| Anemometer Model: MT-4615 Measurement range: 1.40~108.00 km/h Accuracy: 0.80~30.00 m/s |  |
| Thermal imaging camera Model: WB-80VOLTCRAFT® Measurement range: -20 °C - 600 °C Accuracy: ± 2 % ± 2 °C (tested @25 °C) |  |
| Magnetic stirrer Model: SH-2-220V Rotational speed:100–2000 r/min |  |
| Electronic balance Model: BOECO BAS Accuracy: 0.0001 g |  |
| Ultrasonic bath Model: VEVOR Capacity: 6 litres Frequency: 40 kHz |  |

in the FPSC after positive stability inspection of successfully-prepared hybrid nanofluids. Table 3 lists the devices used for measuring thermal conductivity, specific heat, and density of prepared hybrid MWCNT-Al₂O₃ nanomaterials, which belong to the Department of Polymers, University of Miskolc, Hungary. The process of mixing MWCNT-Al₂O₃ nanomaterials into DI water has produced a nanofluid with new thermophysical properties other than those of MWCNT nanowire and Al₂O₃ nanoparticles, which were calculated using Eqs. (2)–(5) [38–41], as indicated in Table 3.

$$\varphi = \left[\frac{\left(\frac{m}{\rho} \right)_{MWCNT-Al_2O_3}}{\left(\frac{m}{\rho} \right)_{MWCNT-Al_2O_3} + \left(\frac{m}{\rho} \right)_{bf}} \right] \times 100 \quad (1)$$

$$C_{p,nf} = \frac{\phi \cdot (\rho_{np} \cdot C_{p,np}) + (1 - \phi) \cdot (\rho_{bf} \cdot C_{p,bf})}{\rho_{nf}} \quad (2)$$

$$\rho_{nf} = \phi \cdot \rho_{np} + (1 - \phi) \cdot \rho_{bf} \quad (3)$$

$$\frac{k_{nf}}{k_{bf}} = \frac{k_{np} + 2k_{bf} + 2\phi(k_{np} - k_{bf})}{k_{np} + 2k_{bf} - \phi(k_{np} - k_{bf})} \quad (4)$$

$$\mu_{nf} = \frac{\mu_{bf}}{(1 - \phi)^{2.5}} \quad (5)$$

2.5. Energy assessment

The thermal efficiency of a FPSC (η_{th}) is the ratio of the thermal energy gained (Q_u) from circulated fluids through tubes to the incident solar radiation (S) and the FPSC effective absorbing area (A_C), according to Eq. (6) [47]. The heat transfer between two bodies with different temperatures produces thermal energy due to heat conduction and convection over a fluid. The thermal energy gain is an important metric for defining the FPSC thermal efficiency, which is influenced by some parameters, such as the fluid mass flow rate, the fluid's thermophysical properties, and the inlet and outlet fluid temperature. Mathematically, Eq. (7) presents this statement [47].

$$\eta_{th,day} = \frac{Q_u}{S A_C} \quad (6)$$

$$Q_u = \dot{m}_f \cdot C_{p,f} (T_{f,out} - T_{f,in}) \quad (7)$$

At sunset, the solar radiation value equals zero (input energy = 0), making the thermal efficiency equal zero, too. However, integrating PCM bags provides a heat source that works as an input energy for the FPSC after sunset. Consequently, the FPSC thermal efficiency during the night could be calculated from Eq. (8) [48], as follows:

$$\eta_{th, night} = \frac{\dot{m}_f \cdot C_{p,f} (T_{f,out} - T_{f,in})}{m_{PCM} \cdot C_{p,PCM} (T_{PCM,i} - T_{PCM,f})} \quad (8)$$

where m_{PCM} , $C_{p,PCM}$, $T_{PCM,i}$, $T_{PCM,f}$ are respectively the total mass of incorporated PCM bags, PCM-specific heat, initial and final PCM temperatures.

In the current study, some thermal parameters that affect the FPSC thermal behaviour, such as heat transfer coefficient, Nusselt number, Reynolds number, friction factor, and pressure drop, were estimated. The Reynolds number of fluid (Re_f) flows inside tubes was estimated using Eq. (9), considering the value of mass flow rate, fluid viscosity, and hydraulic diameter [49].

$$Re_f = \frac{4 \dot{m}}{\pi \mu_f D_h} \quad (9)$$

However, the Nusselt number (Nu_f), which is the ratio of heat convection to heat conduction of fluid flow, was mathematically calculated by Eq. (10) [50]. Besides, the heat transfer coefficient (h) was calculated from Eq. (11) [51]. T_b , T_w and A , calculated by Eq. (12), are the bulk temperature, the tube's wall temperature and the peripheral area of the pipe (Eq. (13)) [51], respectively,

$$Nu_f = h \times \left(\frac{D_h}{K_{nf}} \right) \quad (10)$$

$$h = \frac{\dot{m} C_{p,f} (T_{in,f} - T_{out,f})}{A (T_{avg} - T_w)} \quad (11)$$

$$T_b = \frac{T_{in} + T_{out}}{2} \quad (12)$$



Fig. 3. Preparation procedure of PCM thermal bags.

Table 2
Main thermophysical characteristics of PCM.

| Thermophysical property | value |
|-------------------------------|-------------------------------|
| Thermal conductivity (W/m·K) | 0.21 |
| Specific heat (kJ/kg·K) | 2.1 |
| Transition temperature (°C) | 40-44 |
| Latent heat of fusion (kJ/kg) | 190 |
| Density (kg/m ³) | 380 for liquid, 930 for solid |

The pressure drop (ΔP) is significantly influenced by the friction factor due to the relative increase in circulating fluid's density and can be calculated using Eq. (15) [53].

$$\Delta P = \frac{f \rho L}{2D_{\text{tube}}} \left(\frac{4 \dot{m}}{\rho \pi D^2} \right)^2 \quad (15)$$

2.6. Exergy assessment

The previous subsection discussed the performance of the FPSC based on the law of energy conservation (first law of thermodynamics) to analyse the amount of heat energy entering and exiting the FPSC. This could be achieved by focusing on the quantity of energy produced, considering the heat convection or radiation losses. Besides, the subsection could measure the ability of PCM bags to store heat (quantity) during melting/freezing phases and regarding the effect of nanofluids, finding a heat transfer rate increment with an improvement of FPSC thermal efficiency. However, this subsection evaluates the FPSC performance based on the second law of thermodynamics, considering the energy quality and entropy, focusing on the quality of energy produced, given irrecoverable heat losses to augment useful energy. Accordingly, this section evaluates the effectiveness of PCM to store heat, whether it matches the required energy quality of the FPSC and measures the ability of using nanofluids to reduce entropy and improve the energy utilisation. Thereby, the exergy efficiency will be presented to give the quality of energy relative to the energy supplied from the sun, considering the irreversibility, entropy losses and irregular temperature distribution.

The heat transfer between a hot body (the absorbing plate) and a less hot body (the serpentine tubes and circulated fluid inside) represents the actual work (quality work) of energy produced from the FPSC [54]. The second law of thermodynamics is best represented by the heat conduction and convection between two bodies with different temperatures when they are in thermodynamic equilibrium with the surroundings. Thereby, the thermal exergy produced by the FPSC and exergy destruction are affected by the exergy input (solar exergy) and exergy flow (represented by nanofluids flow and the heat provided by PCM bags), as shown in Fig. 6.

The energy balance equation of the FPSC system was represented by Eqs. (16)-(18) [55].

$$\dot{E}x_{\text{dest}} = \dot{E}x_{\text{heat}} - \dot{E}x_{\text{in}} - \dot{E}x_{\text{out}} - \dot{E}x_{\text{work}} \quad (16)$$

$$\dot{E}x_{\text{dest}} = \sum \left(1 - \frac{T_a}{T_{\text{sun}}} \right) \dot{Q}_s - \dot{W} + \sum m_{\text{in}} \cdot \psi_{\text{in}} - \sum m_{\text{out}} \cdot \psi_{\text{out}} \quad (17)$$

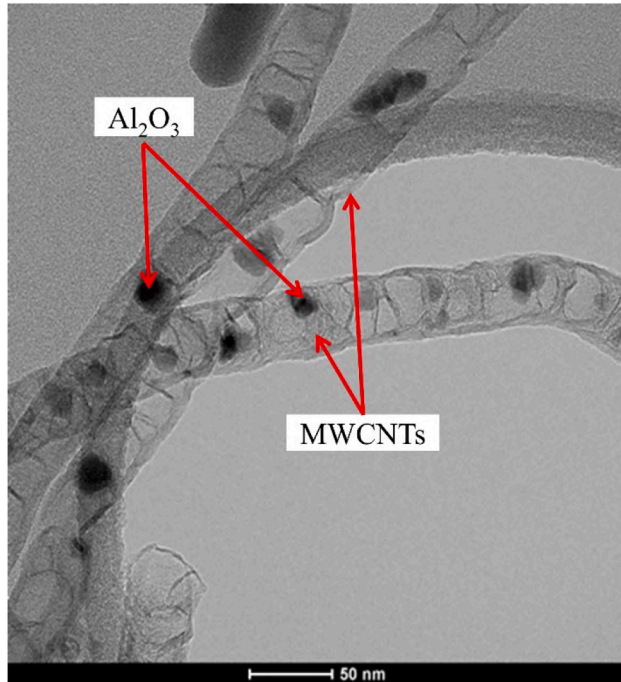


Fig. 4. Surface morphology of MWCNT-Al₂O₃ nanomaterials.

$$A = 2 \times (W + H) l \quad (13)$$

Increasing the volume concentration of dispersed nanomaterials in the base fluid affects the density and viscosity of nanofluid circulation into tubes, increasing the power consumption. Therefore, the friction factor should be calculated in terms of Re number, according to Eq. (14) [52].

$$f_{nf} = (0.79 \ln Re_{nf} - 1.69)^{-2} \quad (14)$$

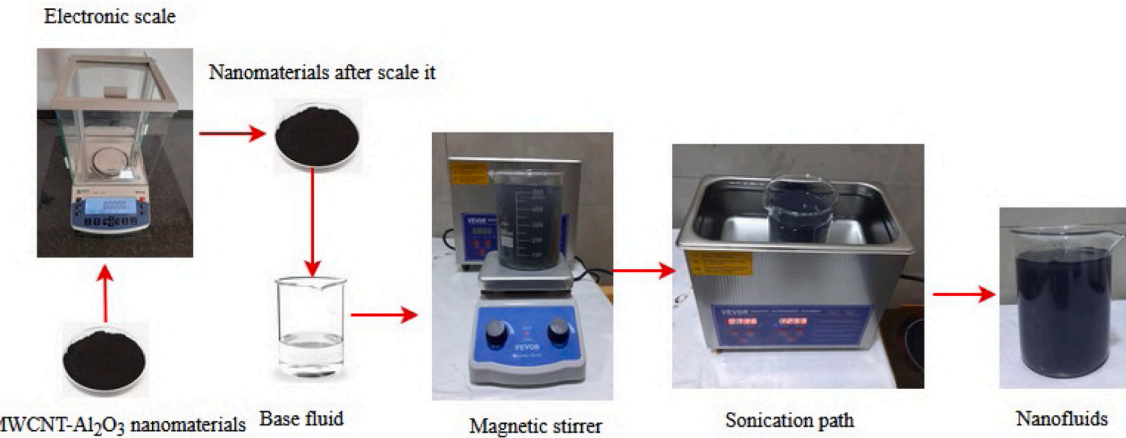


Fig. 5. HNF preparation stages.

Table 3

Thermophysical properties of nanomaterials.

| Property | MWCNT [42,43] | Al ₂ O ₃ [44–46] | MWCNT-Al ₂ O ₃ | Measurement device |
|------------------------------|---------------|--|--------------------------------------|-------------------------|
| Thermal conductivity (W/m·K) | 3000 | 37 | 3031.5 | C-Therm TCi |
| Specific heat (J/kg·K) | 796 | 880 | 951.34 | Mettler-Toledo DSC 823e |
| Density (kg/m ³) | 1600 | 3900 | 3087.91 | (pycnometer A) |
| Colour | Black | White | Black | – |
| Morphology | Nanowires | Nanoparticles | Nanowires- Nanoparticles | – |

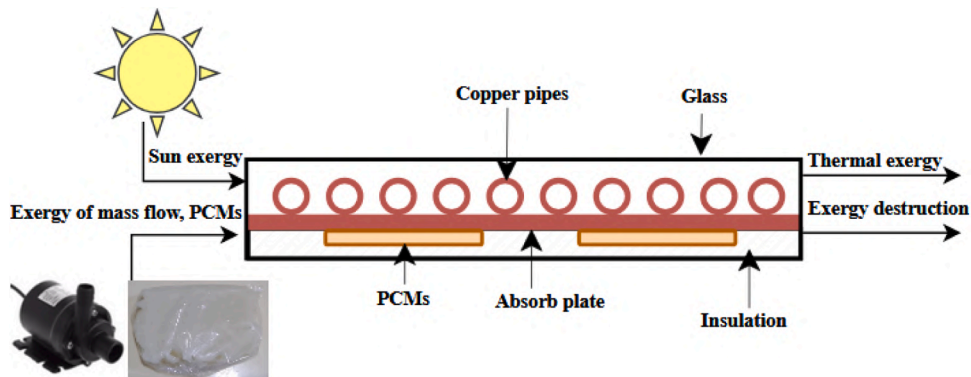


Fig. 6. Control volume of the FPSC.

$$\sum \left(1 - \frac{T_a}{T_{\text{sun}}}\right) \dot{Q}_s - \dot{m} \Delta h - T_a \Delta s = \dot{E}_{\text{dest}} \quad (18)$$

where T_a is the ambient temperature, T_{sun} is the sun temperature (5800 K) [56], and \dot{Q}_s is the absorbed energy by absorbing plate, calculated by Eq. (19) [57].

$$\dot{Q}_s = G_t(\tau\alpha)A_c \quad (19)$$

The change in enthalpy (Δh) and entropy (Δs) of MWCNT- Al₂O₃ nanofluids circulated into the FPSC system could be expressed by Eqs. (20) and (21) [57].

$$\Delta h = h_{\text{out}} - h_{\text{in}} = C_{p,f}(T_{\text{out}} - T_{\text{in}}) \quad (20)$$

$$\Delta s = s_{\text{out}} - s_{\text{in}} = C_{p,f} \ln \frac{T_{\text{out}}}{T_{\text{in}}} - R \ln \frac{P_{\text{out}}}{P_{\text{in}}} \quad (21)$$

Substituting Eqs. (19), (20) and (21) into Eqs. (18) and (17), we can obtain a comprehensive formula of exergy destruction (Eq. (22)), as follows:

$$\dot{E}_{\text{dest}} = \left(1 - \frac{T_a}{T_s}\right) G_t(\tau\alpha)A_c - \dot{m} C_p \Delta T + \dot{m} C_p T_a \left[C_p \ln \left(\frac{T_{\text{out}}}{T_{\text{in}}} \right) - R \cdot T_a \ln \left(\frac{P_{\text{out}}}{P_{\text{in}}} \right) \right] \quad (22)$$

The FPSC exergy efficiency was calculated using Eq. (23). Moreover, the exergy destruction (exergy loss) is a fair metric that helps to calculate the exergy losses and entropy generation of the system (heat transfer losses, and frictions that occurred inside tubes), calculated by Eq. (24) [58].

$$\eta_e = 1 - \frac{S_{\text{gen}} \cdot T_a}{\left[1 - \frac{T_a}{T_{\text{sur}}}\right] \dot{Q}_s} \quad (23)$$

$$\dot{E}_{\text{dest}} = \dot{S}_{\text{gen}} \cdot T_a \quad (24)$$

The sustainability index (SI) is another essential metric derived from the exergy efficiency that could be used to evaluate the solar energy system's effectiveness by reducing the environmental impact. This could be presented mathematically by Eq. (25) [59].

$$SI = \frac{1}{1 - \eta_{ex}} \quad (25)$$

2.7. Uncertainty analysis of measurements

Different devices and instruments have been used for measurements to determine the FPSC performance (listed in Table 1). Throughout the measurements, errors could occur during measurements and implementing an uncertainty analysis of the performed measurements is necessary to specify the potential uncertainty deviation. In this study, experimental uncertainty analysis was performed on the direct measurements, including the inlet and outlet temperature, solar radiation, fluid's specific heat and mass flow rate. The analysis was performed on the FPSC thermal efficiency as an indirect parameter, employing Eq. (26) [60], to ensure the reliability of measured data. Besides, Eqs. (28)-(30) [61] were used to calculate the uncertainty of the energy gain, heat transfer coefficient, and Nusselt number. The FPSC size was neglected, and the parameters denoted by T_{out} , T_{in} , \dot{m} , S , C_p were evaluated according to Eq. (27), in which U is the uncertainty of data measured.

$$\eta_{th} = f(T_{in}, T_{out}, \dot{m}, S, C_p) \quad (26)$$

$$\left[\left(\frac{U_{\eta_{th}}}{U_{\eta_{th}}} \right)^2 \right]_{th} = \sqrt{\left(\frac{U_T}{T_{out}} \right)^2 + \left(\frac{U_T}{T_{in}} \right)^2 + \left(\frac{U_{\dot{m}}}{\dot{m}} \right)^2 + \left(\frac{U_S}{S} \right)^2 + \left(\frac{U_{C_p}}{C_p} \right)^2} \quad (27)$$

The uncertainty of energy gained:

$$\frac{\Delta Q_u}{Q_u} = \sqrt{\left(\frac{\Delta \dot{m}}{\dot{m}} \right)^2 + \left(\frac{\Delta T_i}{T_i} \right)^2 + \left(\frac{\Delta T_o}{T_o} \right)^2} \quad (28)$$

The uncertainty of the heat transfer coefficient:

$$\frac{\Delta h}{h} = \sqrt{\left(\frac{\Delta Q_u}{Q_u} \right)^2 + \left(\frac{\Delta A}{A} \right)^2 + \left(\frac{\Delta T_{avg}}{T_{avg}} \right)^2 + \left(\frac{\Delta T_w}{T_w} \right)^2} \quad (29)$$

The uncertainty of the Nusselt number:

$$\frac{\Delta Nu}{Nu} = \sqrt{\left(\frac{\Delta h}{h} \right)^2 + \left(\frac{\Delta D_h}{D_h} \right)^2} \quad (30)$$

Accordingly, Table 4 shows the uncertainty analysis of parameters discussed above, showing good agreement with the literature studies.

3. Results and discussion

The performance of the developed FPSC was examined in Basra City, Iraq weather conditions during August 2024. The experiments were performed during August from 7:00 to 21:00, for three consecutive days with approximately the same weather conditions, in which the FPSC integrated PCM bags were investigated on the first day, and then modified using HNF with two different concentrations in the following two days. August is generally characterised by high outdoor ambient temperatures and humidity on some days. Besides, the wind speed is changeable throughout the day, reporting fluctuated wind speed between 3.92 and 5.78 m/s during measurements. However, higher values were reported for the average ambient temperature and solar radiation

Table 4
Uncertainty analysis of parameters presented in the current study.

| Parameter | Uncertainty (%) |
|---------------------------|--------------------------|
| Thermal efficiency | 1.09 % |
| Energy gained | 3.02 W |
| Heat transfer coefficient | 9.28 W/m ² .K |
| Nusselt number | 1.38 |

during experimental days, as indicated in Fig. 7. The experiments reported an average of about 500 W/m² at the first hour at 7:00, and maximized gradually attaining a maximum solar radiation of about 1190 W/m² at noon and lowered to zero at sunset around 18:00. The ambient temperature disparity had the same behaviour as solar radiation, recording at the early time about 37.53 °C and then raised to a maximum mark of 49.71 °C at noon. Afterwards, the ambient temperature was gradually decreased to about 37 °C at the end of the experiment at 21:00.

3.1. Energy analysis of FPSCs

3.1.1. Temperature profile

The FPSC outlet temperature is the main metric that has an intrinsic role in controlling the FPSC performance. Thermophysical properties of the circulated fluid, fluid type, mass flow rate, tube design and absorbing plate area remarkably affect the outlet temperature. Fig. 8 displays the FPSC outlet temperature when using the DI water as a working fluid, adding PCM bags at the absorbing plate rear side, and circulating MWCNT-Al₂O₃ at different concentrations. According to the results observed in the figure, fluid circulation into copper tubes helps to absorb heat from the tube walls exposed to direct solar radiation and heat collected by the absorbing plate. This heat energy is then transferred and accumulated into the plastic tank by means of the fluid throughout the operation period. The outlet temperature of the DI water working fluid for the reference FPSC increased gradually at the beginning of the measurements due to the increased ambient temperature and solar radiation, reaching a maximum of 61.3 °C at noon.

Incorporating 10 PCM bags into the FPSC increased the outlet temperature more than the reference FPSC after 9:20. However, the reference FPSC showed higher output temperature in the early morning, attributed to the PCM heat charging phase (melting), which utilised some heat for phase transition. Furthermore, a positive increase in the FPSC outlet temperature using PCM bags, reaching a maximum of 68.6 °C at 12:30. This output temperature is attributed to the heat released by the PCM bags after reaching the full melting phase in the first half of the day, providing additional heat until the end of the day. Consequently, integrating PCM bags has increased the outlet temperature more than that of the reference FPSC, even with sunset, confirming the positive potential of PCM to extend the FPSC productivity after sunset.

Circulating HNFs instead of DI water, along with the PCM bags, has significantly increased the outlet temperature than using PCM bags alone. Improved thermophysical properties of hybrid MWCNT-Al₂O₃ nanomaterials dispersed into DI water enhanced the circulation fluid's thermal properties and positively improved heat convection between

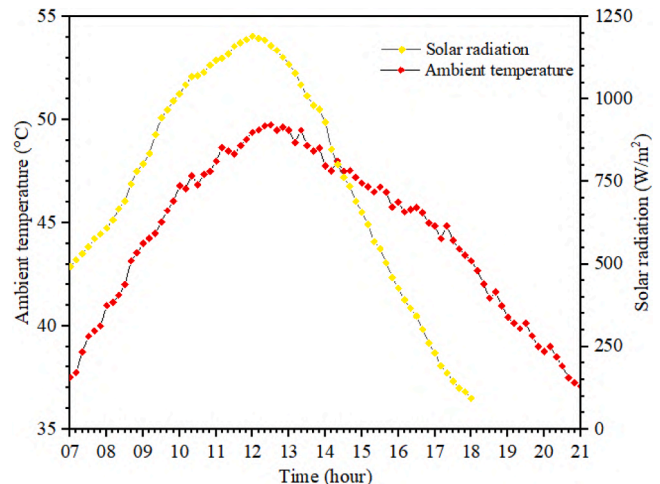


Fig. 7. Climate conditions of the study location during experiments.

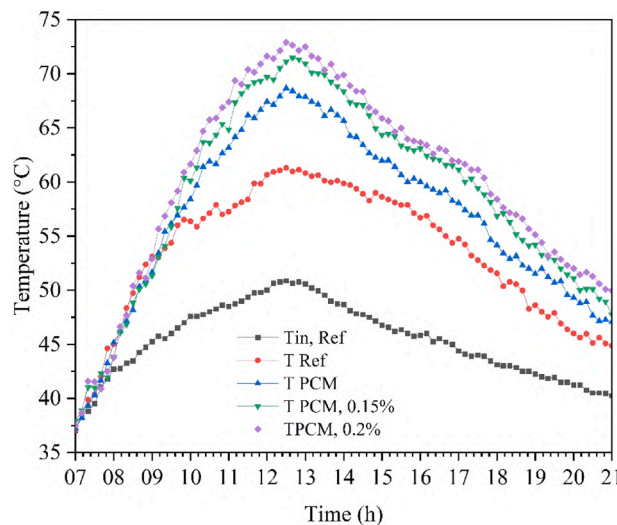


Fig. 8. Outlet temperature of FPSC.

nanofluids and the tube wall. It could be observed from Fig. 8 that the circulation MWCNT- Al_2O_3 at 0.15 % has increased the outlet temperature to a maximum of 71.1 °C at 12:30, while increasing the concentration to 0.2 % attained a maximum FPSC outlet temperature of 72.9 °C. In fact, the conjoint positive effect of PCM and HNFs is reasonable since PCM bags remain in a liquid phase at the midday period, working as a heat source, while HNFs accelerate the heat transfer process. Compared to the reference FPSC, incorporating PCM bags alone has increased the output temperature by 11.9 %, while circulating MWCNT- Al_2O_3 nanofluids at 0.15 %, 0.2 % with the presence of PCM bags indicated an increment by about 16 % and 19 %, respectively.

Water temperature drops rapidly after sunset due to heat losses to the environment. PCM bags have released the latent heat which was stored during the day, maintaining high water temperature after sunset for a certain period. The interesting improvements after sunset could be recognised by maintaining hot water for a longer time than the reference FPSC, with reduced sharp temperature drops and improved thermal efficiency, lowering the dependence on conventional energy sources. Even with gradually reduced water temperature after 17:00, it could be noticed that the heat released from PCM bags has maintained the water with up to 62.89 °C when the volume concentration is 0.2 %, while the FPSC with PCM and reference one has maintained water temperature with about 58 °C and 55.1 °C, respectively.

As earlier indicated, the outer surface temperature variance of FPSCs was inspected by a thermal camera at different times. Thermal photos were indicated for the cases where the FPSC was modified with PCM bags, and that modified with PCM and HNF with 0.2 % concentration at 9:00, 12:00, 15:00 and 18:00 (Fig. 9). In general, it could be noticed that the reference FPSC had a higher outer surface temperature in the first half of the day (at 9:00 and 12:00), while the temperature was increased in the modified FPSCs afterwards (i.e., at 15:00 and 18:00). For instance, Fig. 9 (a) shows that the surface temperature difference between the reference and modified FPSC with PCM bags was 2.1 °C and 3.2 °C at 9:00 and 12:00, respectively. Later on at 15:00 and 18:00, the outer surface temperature of the modified FPSC with PCM bags increased over the reference one by 0.8 °C and 1.6 °C, respectively. Fig. 9 (b) indicates a slight temperature trend regarding the FPSC modified with PCM bags and HNF with 0.2 % concentration. The outer surface temperature of the reference FPSC was higher than that of the modified FPSC by 1.4 °C at 9:00. However, the surface temperature of the modified FPSC was higher than that of the reference FPSC by 0.5 °C at 12:00, 1.6 °C at 15:00 and 1.7 °C at 18:00.

In general, the high surface temperature of the reference FPSC in Fig. 9 at 9:00 could be attributed to the fact that the heat was charged

into the PCM bags during the first day hours. Therefore, it was reasonable to see that the output temperature of the reference FPSC was higher than the modified ones at this time. Afterwards, when the PCM reached a full melting state, the modified FPSCs in all cases were higher than that of the reference one. Such an increment is undoubtedly attributed to the PCM influence as an extra heat source in the modified FPSCs with and without nanofluids. However, the temperature of the modified FPSC with PCM bags and HNF showed a higher outer surface temperature starting from noon. This revealed the influence of HNF, which has expedited the heat charging into PCM to reach a melting state quicker than the bare PCM.

3.1.2. Energy gain and thermal efficiency

The quantity of heat transferred from the FPSC to the plastic tank employing the working fluid represents the thermal energy gain from the system. The energy gain is impacted by the difference between the inlet and outlet fluid temperatures, fluid thermal properties, and its mass flow rate. Fig. 10 illustrates the effect of PCM bags and hybrid MWCNT- Al_2O_3 nanofluids on the useful energy gain of FPSC compared with the average values of reference FPSC. At the beginning of measurements, the reference FPSC showed better energy gain than the modified ones until 9:30, due to the PCM melting process, which lowered the amount of heat transferred to the working fluid. However, the energy gain increased as the PCM reached the full melting state at noon, and extra heat was dissipated to the working fluid. The maximum energy gain verified by reference FPSC was 221.4 W at 12:30, which then lowered as the fluid temperature reduced. On the other side, the insertion of PCM bags helps increase the fluid temperature at noon, leading to increased energy gain compared to the reference FPSC, starting from 10:00. The energy gain was gradually increased encountered with rising fluid temperature to reach a maximum of 277.8 W at 12:40. FPSC with PCM bags achieved an increase in energy gained even with sunset at 18:00, augmenting the energy gain by up to 16.86 % during measurements. Replacement of DI water as a working fluid by the hybrid MWCNT- Al_2O_3 nanofluid resulted in a noticeable change in the energy gain due to enhanced thermal properties. The increased thermal conductivity of fluid due to MWCNT- Al_2O_3 dispersion played a key role in improving heat conduction and convection between circulating fluids, tube wall and absorbing plate, which eventually increased the energy gain. Dispersion of MWCNT- Al_2O_3 nanomaterials with 0.15 % has augmented the energy gain to a maximum of 325.1 W, at 12:40 PM. However, increasing MWCNT- Al_2O_3 concentration to 0.2 % has augmented the FPSC energy gained to a maximum of 341.7 W. Thus compared to the reference collector, the FPSC energy gain was improved by a maximum of 25.8 %, 46.8 % and 54.3 % using PCM bags, PCM bags with MWCNT- Al_2O_3 nanofluid at 0.15 % and 0.2 %, respectively.

Even at a late time, an improvement in the energy gain of the FPSC-integrated PCM bags could be recognised, in which the heat was released due to PCM discharging, confirming an enormous quantity of stored heat during the day. Specifically at 20:00, the energy gain attained was 138.34 W under hybrid nanofluid at volume concentration 0.2 % and PCM bags, while incorporating PCM bags achieved an energy gain of about 118.75 W, compared with 80.1 W attained by the reference FPSC. The improved energy gain is attributed to the ability of PCM bags during the discharging phase, which continues releasing heat after sunset, in addition to the hybrid nanomaterials, which increased the heat transfer coefficient and improved the energy gain.

Thermal efficiency is an intrinsic metric to evaluate the FPSC performance, which is the ratio of output energy (useful energy gain) to the input energy in terms of incident solar radiation and FPSC area. Fig. 11 displays the thermal efficiency of FPSCs under the influence of PCM bags and hybrid MWCNT- Al_2O_3 nanofluids at different concentrations. At the beginning of the experimental days, the reference FPSC displayed a better thermal efficiency than the FPSC improved by PCM bags and HNFs, until around 9:30. This negative behaviour is attributed to the low heat energy gain of modified FPSCs during the PCM heat charging phase,

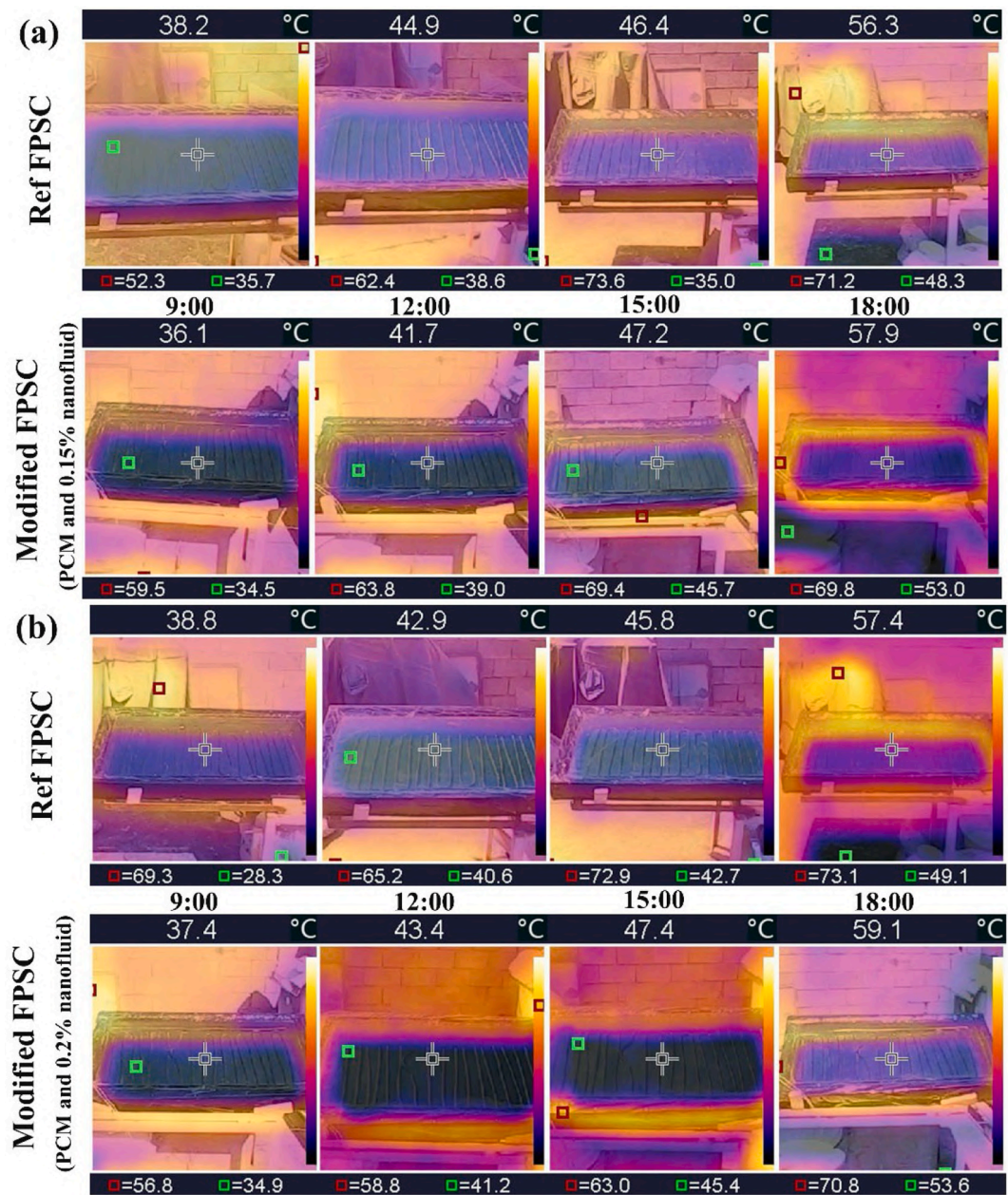


Fig. 9. Thermal photos of the reference FPSC compared with the FPSC modified with (a) PCM bags, (b) PCM bags and 0.2 % HNF.

as stated earlier. However, the thermal efficiency was gradually increased right after 9:40 for the modified FPSC with PCM bags, achieving a maximum of 48.1 %, compared to 43.7 % for the reference FPSC. Employing MWCNT-Al₂O₃ nanofluids with PCM bags in the FPSC led to a remarkable increase in thermal efficiency even after sunset. The maximum thermal efficiency calculated for the modified FPSCs was about 52.8 % and 54.9 % at 0.15 % and 0.2 % concentrations, respectively. Conclusively, the combined effect of PCM (as an extra heat input energy) and HNFs (as a heat carrier) has enhanced the thermal efficiency of the FPSC until the end of the experiments. Moreover, the PCM bags were releasing heat through the discharging phase even under lower temperatures, enhancing the thermal efficiency of the FPSC. For instance, at 18:00, the measured thermal efficiency was 24 %, 21.98 %, 19.51 % for the FPSC with PCM and 0.2 % HNF, PCM only and reference case, respectively. Accordingly, incorporating PCM bags and hybrid nanofluids has maintained high thermal efficiency throughout the measurements, which approved the effectiveness of using PCM bags as a

heat source at sunset and the feasibility of HNF for increased thermal efficiency.

3.1.3. Effect of volume fractions on nusselt number and heat transfer coefficient

Thermal parameters such as Nusselt number, heat transfer coefficient, Reynolds number, and pressure drop are key indicators in evaluating the FPSC performance. Nanoparticle dispersion is proven to enhance the thermal performance of the base fluid thanks to the advanced new thermophysical properties. Fig. 12 and Fig. 13 display the effect of using PCM bags and HNFs on the Nusselt number and heat transfer coefficient at different concentrations against the base fluid over time. It could be observed in the figure that the Nusselt number and heat transfer coefficient were increased as the concentration of MWCNT-Al₂O₃ nanomaterials dispersed into water increased.

Nanofluids are characterised by higher thermal conductivity than conventional fluids due to the enlarged area of solid nanoparticles

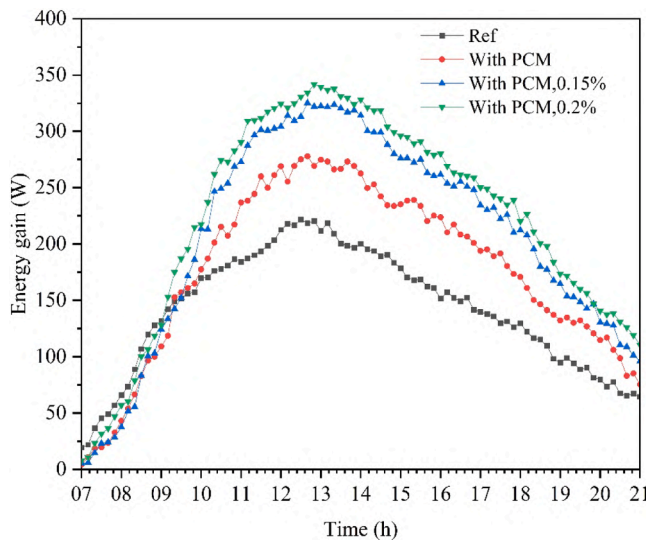


Fig. 10. Energy gain of FPSCs with PCM bags and HNFs.

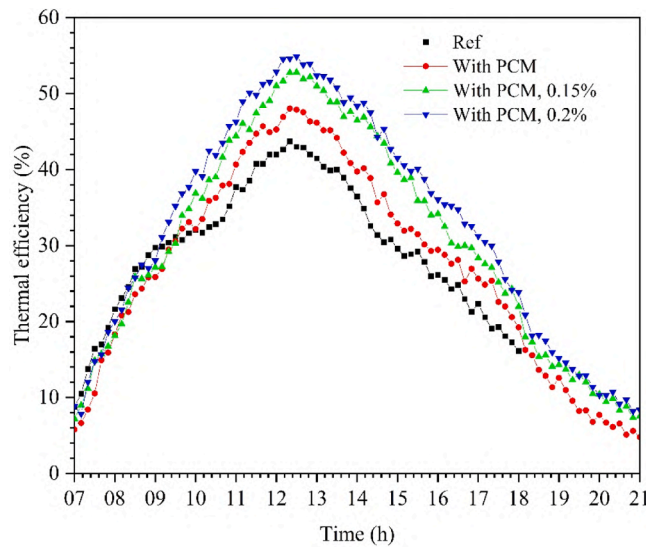


Fig. 11. Thermal efficiency of FPSCs with PCM bags and HNFs.

suspended, which improves thermal conductivity which increasing the heat transfer coefficient and Nusselt number. However, integrating PCM bags on the rear side of FPSC has augmented the Nusselt number specifically through the discharging period that released heat towards the absorbing plate, then to the tubes that have nanofluid. The temperature difference between the absorbing plate and HNF may temporarily decrease at the PCM melting phase in the morning, since the heat is inside the PCM bags. Therefore, the Nusselt number is affected by the heat charging and discharging to/from PCM bags. During heat charging, the heat is continuously absorbed from the absorbing plate and utilised to convert the solid PCM to liquid, causing a slight decrease in the heat transfer to the nanofluid and leading to a slight decrease in the Nu number. Similarly, the PCM bags release heat to the tubes during the heat discharging phase, providing a higher temperature difference, which improves the heat transfer and the Nusselt number. However, the PCM-based FPSC showed poor performance in the beginning hours since part of the FPSC heat was charged into the PCM bags during the melting phase at the beginning, affecting the Nusselt number and heat transfer coefficient values even when HNFs were employed. The outlet temperature and thermal conductivity of HNFs have significantly influenced

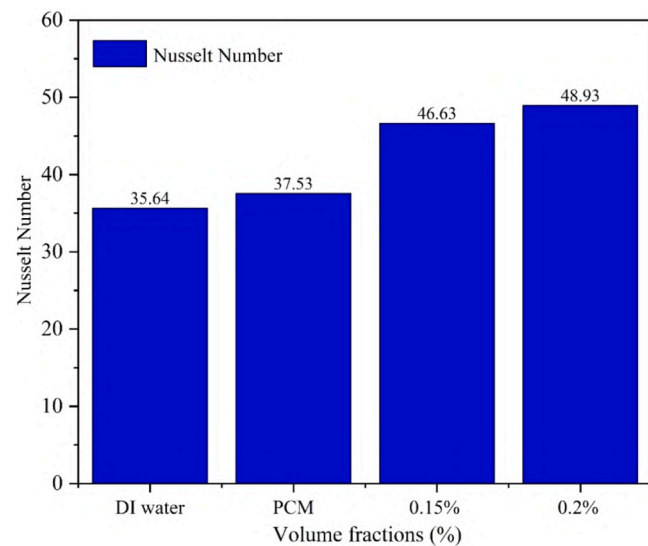


Fig. 12. Nusselt number of FPSCs with PCM bags and HNFs.

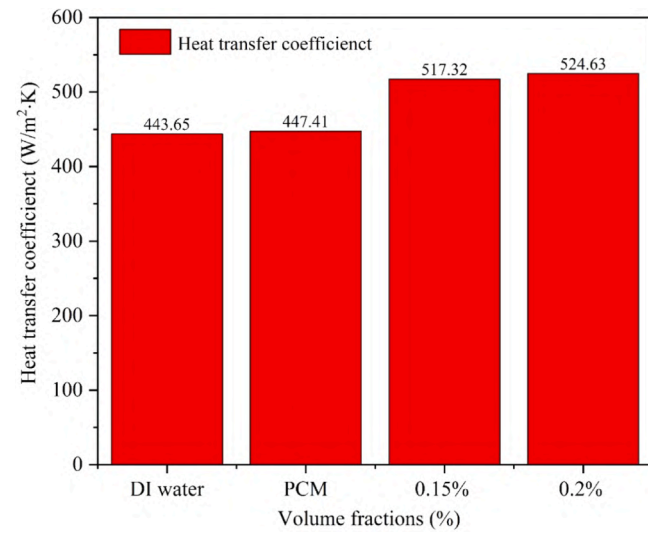


Fig. 13. Heat transfer coefficient of FPSCs with PCM bags and HNFs.

the Nusselt number and heat transfer coefficient, which were gradually increased in the midday (maximum at noon) and reduced at low outlet temperatures. A slight Nusselt number variation of about 37.53 using PCM bags, against 35.64 calculated for the reference one. Fig. 13 shows the influence of using PCM bags and HNF at different volume concentrations on the heat transfer coefficient. Similar behaviour is remarked for the Nu number during heat charging and discharging to/from the PCM bags during the day and sunset. Integrating PCM bags has achieved stable water temperatures and increased heat transfer coefficient during low solar radiation till sunset, while the HNF improve heat transfer of fluid flow. The maximum heat transfer coefficient of the modified FPSC with PCM bags was about 447.41 W/m²·K, while the reference FPSC indicated a maximum of 443.65 W/m²·K due to growing outlet temperature with PCM incorporation. Employing hybrid nanomaterials has improved the thermal performance of FPSC, increasing the Nusselt number by a maximum of 46.63 and 48.93 at 0.15 % and 0.2 % concentrations, respectively. Besides, the heat transfer coefficient was also improved with increased nanofluid concentration, reaching a maximum of 517.32 and 524.63 W/m²·K, when increasing the MWCNT-Al₂O₃ nanomaterials concentration from 0.15 % to 0.2 %. Conclusively, HNFs have a direct effect on raising the heat transfer coefficient due to

improved thermal conductivity and enhanced heat convection. Besides, PCM bags worked to balance the heat transfer coefficient and improved the heat transfer coefficient of the fluid, which eventually improved the FPSC performance.

3.1.4. Pressure drop of HNFs

Despite the advanced FPSC thermal efficiency using nanofluids more than the base fluid, increasing hybrid nanomaterial concentration has increased pressure drop due to increased nanofluid density, even with increased Reynolds numbers. Pressure drop is significantly affected by the friction factor due to the increased volume concentration of dispersed nanomaterials. Besides, the Reynolds number was also influenced by increased viscosity of the circulated HNF. Fig. 14 demonstrates that the pressure drop increased with increased Reynolds number and HNF concentration. However, the FPSC indicated a low-pressure drop using DI water as a base fluid due to its low density compared with the nanofluids. A slight pressure drop difference could be observed when using PCM bags, compared to the reference FPSC. The maximum pressure drop recorded for the nanofluid at 0.2 % concentration was 36.47 Pa, while it was 35.96 Pa at 0.15 %, and 29.71 Pa when the DI water was employed. Increased pressure drop has a negative effect on pumping power since more power is required to circulate the working fluids into tubes, due to increased density and friction between nanomaterials and internal tube walls.

3.2. Exergy analysis for FPSCs

3.2.1. Exergy efficiency

The FPSC exergy efficiency is typically improved by enhancing the heat transfer between the inner tube's wall attached to the absorbing plate by heat conduction and circulating fluids by heat convection. The synthesised MWCNT-Al₂O₃ nanomaterials have higher thermophysical properties than single nanomaterials, increasing the thermal conductivity and specific heat of the HNFs significantly. As a result, the Nusselt number and heat transfer coefficient of the nanofluid will increase the heat absorption from the PVT and augment the outlet temperature. The FPSC exergy efficiency is affected by several factors, such as the entropy generation, absorbed energy and ambient temperature, as indicated in Eq. (23). Consequently, the changes in enthalpy and entropy are mainly impacted by the thermophysical properties of the circulated fluid and temperature difference through the measurement, affecting the FPSC exergy efficiency. Fig. 15 demonstrates the variations of FPSC exergy efficiency applying PCM bags and hybrid MWCNT-Al₂O₃ nanofluids at different concentrations compared to the reference PVT.

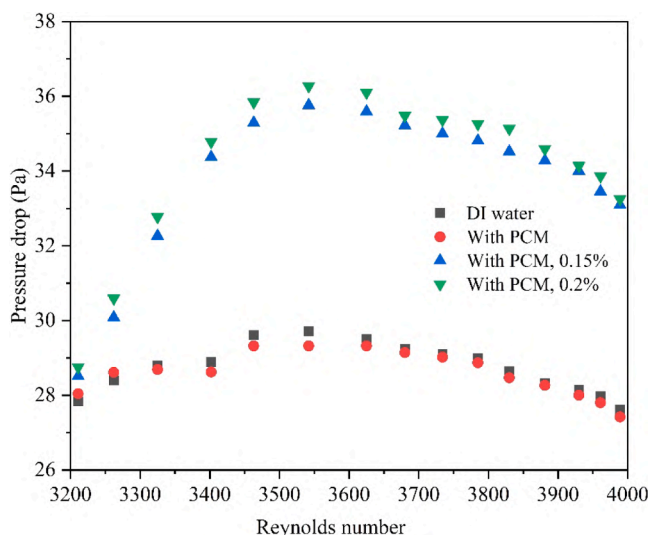


Fig. 14. Pressure drop of FPSCs at various Reynolds Numbers.

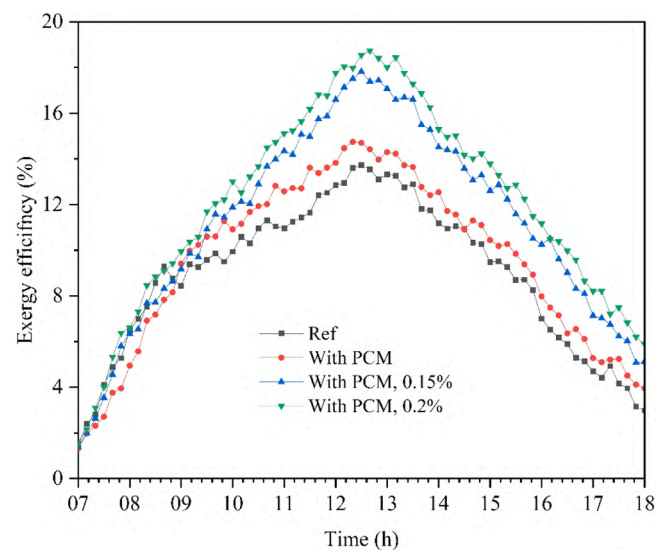


Fig. 15. Exergy efficiency of the FPSC with PCM bags and HNFs.

In the earlier morning hours, the PCM absorbs heat from the absorbing plate surface, reducing the temperature difference between the FPSC and the surrounding environment for a period of time, which temporarily reduces exothermic losses. The reference FPSC accomplished a slightly higher exergy efficiency temporarily than the one integrated PCMs bags/PCM bags and HNF due to the PCM charging phase, which stored heat in a latent form. After 8:40, the PCM bags with HNF at 0.2 % achieved a remarkable increase compared with the other cases, thanks to the stable temperature from the absorbing plate at PCM melting temperature, which reduces temperature fluctuations and heat losses. As a result, nanofluids help lower heat losses due to thermal resistance within the FPSC and increase the excitation efficiency of the FPSC, while the heat transfer coefficient reduces the thermal gradients within the collector layers. As could be observed from the figure, employing hybrid MWCNT-Al₂O₃ nanofluids with PCM bags achieved the highest FPSC performance. Explicitly, dispersing 0.2 % of MWCNT-Al₂O₃ hybrid nanomaterials into water has increased the FPSC exergy efficiency by 18.73 %. However, the FPSC exergy efficiency was about 17.81 % when 0.15 % of hybrid MWCNT-Al₂O₃ was employed with the PCM bags. Besides, PCM bags showed an exergy efficiency of about 14.74 %, while the reference FPSC attained 13.57 %. Correspondingly, it could be concluded that the FPSC exergy efficiency was augmented by about 8.6 %, 31.2 %, and 38 % when employing PCM bags, PCM bags and hybrid MWCNT-Al₂O₃ nanofluids at 0.15 %, and 0.2 %, respectively, over the reference case. During the heat discharging from PCM bags, the stable heat release helped the FPSC to attain higher-quality thermal efficiency, while providing heat to the circulating nanofluid has raised the exergy efficiency over the reference FPSC.

The outcomes of this work are remarkable compared with the literature studies, as indicated in Table 5. As could be recognised, the output water temperature, thermal and exergy efficiencies are on average higher than those of most literature studies. This may indicate the remarkable role of combining PCM and hybrid nanofluids to augment the FPSC thermal performance regardless of collector size and design.

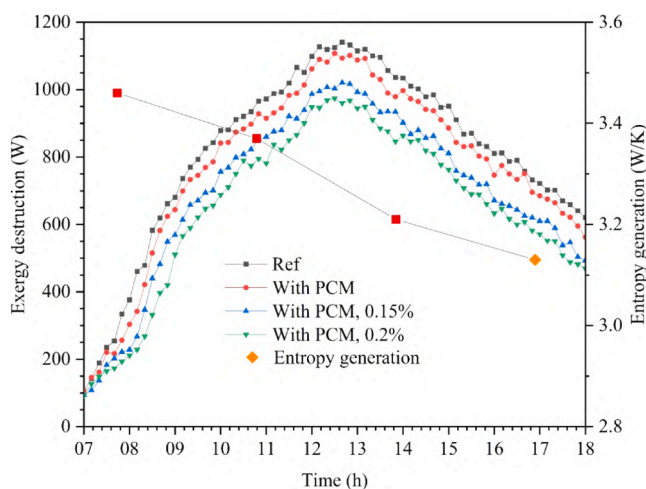
3.2.2. Entropy generation and exergy destruction

Fig. 16 displays the exergy destruction and entropy generation through the measurements using PCM and MWCNT-Al₂O₃ nanofluids at different concentrations. Imperfect conductive heat transfer from the tube surface (attached over the absorbing plate) and circulating nanofluid by convection from one side, and the friction generated between nanoparticles to the pipe walls from the other side leads to entropy generation within the FPSC. The exergy destruction and entropy

Table 5

Comparison of the current study with recent literature studies in terms of output water temperature, thermal and exergy efficiencies.

| Ref. | Study location | FPSC area (m ²) | Improvement method | Output water temperature (°C) | Thermal efficiency (%) | Exergy efficiency (%) |
|---------------|-------------------|-----------------------------|---|-------------------------------|------------------------|-----------------------|
| [62] | Hyderabad, India | 3 | MWCNT/water nanofluid | — | 52.4 | 2.67 |
| [63] | Mansoura, Egypt | 0.905 | PCM channels | 53 | 34.9 | 24.79 |
| [64] | Sharjah, UAE | 0.85 | Si ₃ N ₄ /water nanofluids | 55 | 8 | — |
| [65] | Jabalpur, India | 0.74 | Eutectic PCMs | 85.6 | 15.45 | — |
| [66] | Coimbatore, India | 2 | MWCNT/SiO ₂ -enhanced PCM | 70 | 5.7 | — |
| [67] | Simulation input | — | Al ₂ O ₃ , Cu, MWCNT, SiO ₂ -based single and HNFs | 61.3°C-83.2°C | 40.6 %-70.4 | — |
| Current study | Basra city, Iraq | 0.5 | PCM bags + MWCNT- Al ₂ O ₃ /water HNF | 72.9 | 25.6 | 38 |

**Fig. 16.** Exergy destruction and entropy generation.

generation are factors that have a vital role in determining the exergy efficiency of the FPSC system. Therefore, dropping these factors is essential to improve the efficiency of the thermal system. Nevertheless, in exergy analysis, it's necessary to determine the exergy destruction and impact of using PCM bags and nanofluids to reduce the exergy destruction and improve the exergy performance of the thermal system. Referring to Fig. 16, it could be observed that replacing DI water with PCM bags and MWCNT-Al₂O₃ nanofluids has reduced the exergy destruction more than using DI water and PCM bags alone. The reference FPSC have higher exergy destruction in the early morning, recording 644 W at 9:00, with entropy generation of 3.25 W/K. In contrast, employing PCM bags has reduced the exergy destruction to about 624 W, along with entropy generation reduction to 3.23 W/K. Besides, circulating nanofluid at 0.2 % along with PCMs bags has reduced the exergy destruction and entropy generation to 461 W and 3.15 W/K, respectively. Improved thermal conductivity of HNF has reduced the temperature gradient in the FPSC and increased the heat transfer coefficient, leading to a reduction in the entropy generation and irreversible losses. Moreover, the heat charging phase of PCM has reduced the temperature difference between the tube wall surface and HNF, reducing the entropy generation for an extended period. This could be attributed to the enhanced thermal properties of circulating nanofluids and the additional heat supply of PCM bags. Maximum exergy destruction and entropy generation calculated for the FPSC with DI water were 1140.79 W and 3.46 W/K, respectively, which then reduced to 974.19 W and 3.13 W/K at 0.2 % MWCNT- Al₂O₃ HNF and 1020.61 W and 3.21 W/K at 0.15 %. Therefore, increased nanomaterials achieved lower exergy destruction and entropy generation due to increased heat gain of circulated nanofluids, which augmented the outlet temperature even with a constant flow rate. Thereby, a decrement in the FPSC irreversibility occurred due to the enhanced heat transfer coefficient.

Thereby, using PCMs bags and HNF has significantly reduced the exergy destruction and entropy generation, which increased the exergy efficiency and improved the FPSC performance.

3.2.3. Sustainability index

The sustainability index (SI) metric is a vital indicator to measure the development of a system towards environmental sustainability. However, this index is limitedly discussed in literature studies dealing with solar energy systems. In the current research, the SI was calculated using Eq. (25) considering the FPSC exergy efficiency for the reference system and that integrated with PCM bags, and with PCM bags and nanofluids at 0.15 % and 0.2 %. The calculation results displayed that the maximum SI achieved was 1.23 when applying MWCNT- Al₂O₃ HNF at 0.2 % with applied PCM bags, followed by the case of using 0.15 %, attaining an SI of 1.21. Besides, employing PCM bags at the FPSC rear side with water circulation achieved 1.17, while the reference FPSC system attained 1.14. Correspondingly, the SI of the FPSC integrated with PCM bags, PCM and MWCNT- Al₂O₃ HNF with 0.15 % and 0.2 % was maximised to 2.6 %, 5.2 %, and about 7 %, respectively.

3.3. Economic analysis of improved FPSC by PCMs and HNFs

The economic analysis of FPSC-integrated PCM bags and HNFs helps specify the payback period and determine the effective cost of improvements proposed [68]. In the current work, the daily maintenance (which is not necessarily conducted daily during the operation period) and operational costs (including the water pump, flow sensors, etc.) are significant parameters to calculate the economic feasibility. On the other hand, the synthesised hybrid nanomaterials help reduce the cost thanks to their superior purity compared to that purchased from companies. Therefore, the cost of HNFs delivered to the FPSC for each operation day is determined by dividing the total price by year days. In other words, the daily cost of the circulated nanofluids is estimated by dividing the overall price (raw nanomaterial and their preparation) by 365 operation days [69]. The net profit was calculated by Eq. (28) considering the cost of all FPSC parts (shown in Table 6), including the reference and

Table 6

Cost of FPSCs, including that of PCM bags and HNFs.

| Cost aspect | Reference FPSC | FPSC integrated PCM | FPSC integrated PCM and HNF |
|-------------------------------|----------------|---------------------|-----------------------------|
| Configuration (IQD) | 215,000 | 215,000 | 215,000 |
| Maintenance (IQD/day) | 5.13 | 6.82 | 8.61 |
| Operation cost (IQD/day) | 4.67 | 4.67 | 5.11 |
| PCM (IQD/day) | — | 4500 | 4500 |
| Nanofluids (IQD/day) | — | — | 226.63 |
| Energy productivity (IQD/day) | 303.71 | 387.87 | 483 |
| Net profit | 293.91 | 372.26 | 394.56 |
| Payback period (days) | 731.51 | 577.55 | 544.9 |

improved FPSC with their accessories (wooden blocks, galvanized plate, plastic tanks, plastic containers, pipes, coils, glass, insulations, absorbing plates, etc.).

$$\text{Net profit} = \text{Energy production cost} - \text{Fluids/PCM cost} - \text{Operation Cost} - \text{Maintenance cost} \quad (31)$$

To estimate the cost of FPSC thermal energy productivity, the thermal energy produced from a typical electric water heater is about 3000 W for one day, with 15 operation hours was considered. The cost of heating water produced by an electric water heater is calculated according to the kWh specified by the Ministry of Electricity, Iraq, considering the operation time of the produced energy obtained in a day, multiplied by the electricity tariff [70].

Referring to the above equations and data of Table 6, the FPSC improved using 0.2 % MWCNT-Al₂O₃ nanofluids and PCM bags achieved a payback period of about 545 days, thanks to maximised thermal energy productivity with a difference of about 32 days when employing PCM bags alone. However, the reference FPSC achieved a payback period of about 732 days, confirming the feasibility of employing PCM and HNFs to improve the FPSC performance from energetic, exergetic and economic points of view.

4. Limitations, challenges, and future studies

Regardless of the remarkable advancements achieved for the FPSC employing PCM and HNF, the current work has encountered some technical challenges. These issues are mainly associated with the incorporation method of PCM bags into the FPSC, with an optimal way to guarantee even heat charging and discharging cycles. Therefore, flexible thermal bags have been utilised for this purpose. However, these bags may influence the heat transfer rate to and from the PCM since they are basically made from nylon, of poor thermal conductivity. Besides, long-term operation is not guaranteed for such PCM carriers. On one hand, some PCM types could be expensive, especially when packaged into special bags with no leakage is another challenge of this work, since it has health and environmental concerns. On the other hand, nanofluid cost and its preparation method are rather expensive and a complex strategy and still under research when it comes to long-term operation. Nanofluid safe transportation, agglomeration/sedimentation and decreased efficiency over time are other limitations that need to be tackled.

Regardless of the remarkable advancements achieved for the FPSC employing PCM and HNF, and the above limitations and challenges, several research insights could be proposed for future studies, as follows:

- Different design configurations could be analysed to install PCM bags into the FPSC with optimised PCM quantity and the best connection of absorbing plate and fluid pipes to reduce heat losses.
- Other PCM types, preferably Bio-based PCMs, could be explored to ensure safe operation for the long term. Besides, low-cost nanofluid types could also be investigated to quantify the thermal advancements.
- Diverse absorbing layer designs could be investigated instead of the flat one to augment the heat transfer rate, such as the corrugated and zigzag absorbers.
- Incorporating nanoparticles into the PCM could be investigated, although this technique has some preparation and stability concerns [23]. Modern nano-PCM preparation techniques could be adopted in this regard.
- Other enhancers, such as fins, could be introduced along with the PCM and nanofluids to further indicate the overall thermal improvement of the three enhancers. Fins could also be explored with different shapes and designs, such as zigzag [71], root-like [72], louvre [73], and so on, since they showed remarkable advancements.

However, the system's complexity and economic aspects are very important in such studies.

- The environmental shortcomings need to be included in future studies to highlight and quantify the environmental advantages of such modified systems.

5. Conclusions

The present research was conducted to evaluate the thermal advances on a flat plate solar collector (FPSC) employing phase change material (PCM) bags and circulating MWCNT-Al₂O₃ hybrid nanofluid (HNF) with 0.15 % and 0.2 % concentrations. The PCM was placed individually on the rear of the absorbing plate, while the HNF was circulating inside serpentine pipes, unlike nano-enhanced PCM techniques. The experimental rig was designed and examined under severe hot weather conditions in Basra City, Southern Iraq. Multiple energy, exergy and economic aspects were considered to show a techno-economic analysis of the proposed system. The findings achieved in the present work led to the following conclusions:

1. Overall, employing PCM bags has increased the output temperature of the FPSC compared to the reference FPSC without PCM. However, the output temperature of the FPSC enhanced with PCM declined slightly in the first hours of the day since part of the heat was used to melt the PCM until it reached the full melting temperature. The productivity was maximised further by employing the HNF at various concentrations along with the PCM inclusion.
2. The energy gain of FPSC was enhanced by a maximum of about 26 %, 47 % and 54 % using PCM bags, and PCM bags with MWCNT-Al₂O₃ nanofluid at 0.15 % and 0.2 %, respectively.
3. The maximum thermal efficiency calculated for the modified FPSCs has increased by 10 %, 20.8 % and 25.6 %, using PCM, and PCM with HNF at 0.15 % and 0.2 % concentrations, respectively.
4. FPSC exergy efficiency was augmented by about 9 %, 31 %, and 38 %, respectively, when employing PCM, and PCM with MWCNT-Al₂O₃ HNFs at 0.15 % and 0.2 %, over the reference case.
5. The sustainability index of the FPSC was improved by up to 3 %, 5 %, and 7 % when integrating PCM, PCM with MWCNT-Al₂O₃ HNFs at 0.15 % and 0.2 %, respectively, over the reference case.
6. Economic analysis showed that the payback period of the FPSC could be reduced by about 21 % and 25 %, employing PCM and PCM with MWCNT-Al₂O₃ HNFs at 0.2 % concentration, respectively.

CRediT authorship contribution statement

Mohammed Alktranee: Writing – original draft, Investigation, Formal analysis, Data curation. **Qudama Al-Yasiri:** Writing – original draft, Investigation, Formal analysis, Data curation. **Mushtaq A. Al-Furaiji:** Writing – review & editing, Formal analysis, Data curation, Conceptualization. **Hassan A. Hameed Al-Hamzawi:** Writing – original draft, Investigation, Data curation. **Péter Bencs:** Writing – review & editing, Supervision, Project administration, Conceptualization, Funding acquisition. **Márta Szabó:** Supervision, Project administration, Funding acquisition, Formal analysis.

Declaration of competing interest

The authors declare that they have no known competing financial interests or personal relationships that could have appeared to influence the work reported in this paper.

Acknowledgement

This research was supported by the EKÖP-24-4-I through the Hungarian consortium EISZ and the Elsevier agreement.

Data availability

Data will be made available on request.

References

- [1] S.A. Awuku, A. Bennadji, F. Muhammad-Sukki, N. Sellami, Public-private partnership in Ghana's solar energy industry: the history, current state, challenges, prospects and theoretical perspective, *Energy Nexus*. 6 (2022) 100058, <https://doi.org/10.1016/j.nexus.2022.100058>.
- [2] K. Obaideen, A.G. Olabi, Y. Al Swailmeen, N. Shehata, M.A. Abdelkareem, A. H. Alami, et al., Solar energy: applications, trends analysis, bibliometric analysis and research contribution to sustainable Development Goals (SDGs), *Sustainability*. 15 (2023) 1418, <https://doi.org/10.3390/su15021418>.
- [3] Shahad Mohammed Radhi, Sadeq Al-Majidi, H.A.R. Maysam Abbod, Predicting solar power generation utilized in Iraq power grid using neural network, *Misan J Eng Sci* 3 (2024) 38–62, <https://doi.org/10.61263/mjes.v3i1.72>.
- [4] M.A. García-Rincón, J.J. Flores-Prieto, Nanofluids stability in flat-plate solar collectors: a review, *Sol. Energy Mater. Sol. Cells* 271 (2024) 112832, <https://doi.org/10.1016/j.solmat.2024.112832>.
- [5] M. Ghazy, A.E. Zohir, E.S. Ali, A.S. Alsaman, A.M. Farid, H.H. El-Ghetany, et al., State-of-the-art-solar energy-driven adsorption desalination systems, *Energy Nexus*. 15 (2024) 100319, <https://doi.org/10.1016/j.nexus.2024.100319>.
- [6] S.A. Kadhim, K.A. Hammoodi, H.M. Ali, F.L. Rashid, H. Togun, A.M. Alsayah, et al., Influence of the typical twisted tape inserts into the inner tube of double-pipe heat exchanger: a limited review, *Results. Eng.* 25 (2025) 104386, <https://doi.org/10.1016/j.rineng.2025.104386>.
- [7] A.A. Hachicha, Z. Said, Numerical modeling and multi-objective optimization of direct absorption solar collectors using mono and hybrid nanofluids, *J. Clean. Prod.* 414 (2023) 137740, <https://doi.org/10.1016/j.jclepro.2023.137740>.
- [8] S. Li, X. Gong, W. Lin, Y. Sun, Z. Ma, Review of transpired solar collectors: heat and mass transfer mechanisms and enhancement, system integration, and performance assessment and optimisation, *J. Clean. Prod.* 450 (2024) 141967, <https://doi.org/10.1016/j.jclepro.2024.141967>.
- [9] A. Kumar, R. Maithani, M.A. Ali, N.K. Gupta, S. Sharma, T. Alam, et al., Enhancement of heat transfer utilizing small height twisted tape flat plate solar heat collector: a numerical study, *Case Stud. Therm. Eng.* 48 (2023) 103123, <https://doi.org/10.1016/j.csite.2023.103123>.
- [10] K.A. Hammoodi, I.A. Abdulghafor, S.A. Kadhim, A. Elsheikh, D.R. Nayyaf, A. mohsin Alsayah, et al., Effect of air layer on PCMs melting process inside a spherical container: a numerical investigation, *Results. Eng.* 24 (2024) 103088, <https://doi.org/10.1016/j.rineng.2024.103088>.
- [11] Ceylan İ, Gürel AE, A. Ergün, Guma Ali İH, Ağbülü Ü, G. Yıldız, A detailed analysis of CPV/T solar air heater system with thermal energy storage: A novel winter season application, *J. Buil. Eng.* 42 (2021) 103097, <https://doi.org/10.1016/j.jobe.2021.103097>.
- [12] H. Al-Lami, D.S.J. Al-Saeedi, A.A.H. Almaidi, Q. Al-Yasiri, Conjoint effect of nanofluids and baffles on a heat exchanger thermal performance : numerical approach, *Misan. J. Eng. Sci.* 3 (2024) 137–155, <https://doi.org/10.61263/mjes.v3i2.105>.
- [13] A. Haleem, M. Javaid, R.P. Singh, S. Rab, R. Suman, Applications of nanotechnology in medical field: a brief review, *Glob. Heal. J.* 7 (2023) 70–77, <https://doi.org/10.1016/j.glohj.2023.02.008>.
- [14] C. Venkateswara Raju, C. Hwan Cho, G. Mohana Rani, V. Manju, R. Umapathi, Y. Suk Huh, et al., Emerging insights into the use of carbon-based nanomaterials for the electrochemical detection of heavy metal ions, *Coord. Chem. Rev.* 476 (2023) 214920, <https://doi.org/10.1016/j.ccr.2022.214920>.
- [15] M.S. Aljibory, PDBJ Alsulayfani, PDMN. Mahmood, Improvement of concrete mechanical properties by adding nanomaterials, *Misan J. Eng. Sci.* 2 (2023) 57–70, <https://doi.org/10.61263/mjes.v2i2.62>.
- [16] R. Umapathi, C.V. Raju, M. Safarkhani, J. Haribabu, H.U. Lee, G.M. Rani, et al., Versatility of MXene based materials for the electrochemical detection of phenolic contaminants, *Coord. Chem. Rev.* 525 (2025) 216305, <https://doi.org/10.1016/j.ccr.2024.216305>.
- [17] G. Paramasivam, V.V. Palem, S. Meenakshy, L.K. Suresh, M. Gangopadhyay, S. Antherjanam, et al., Advances on carbon nanomaterials and their applications in medical diagnosis and drug delivery, *Colloids Surf. B Biointerfaces* 241 (2024) 114032, <https://doi.org/10.1016/j.colsurfb.2024.114032>.
- [18] G.M. Rani, C-M Wu, K.G. Motora, R. Umapathi, CRM. Jose, Acoustic-electric conversion and triboelectric properties of nature-driven CF-CNT based triboelectric nanogenerator for mechanical and sound energy harvesting, *Nano Energy* 108 (2023) 108211, <https://doi.org/10.1016/j.nanoen.2023.108211>.
- [19] M.A. Subhan, K.P. Choudhury, N. Neogi, Advances with molecular nanomaterials in industrial manufacturing applications, *Nanomanufacturing* 1 (2021) 75–97, <https://doi.org/10.3390/nanomanufacturing1020008>.
- [20] R. Umapathi, M. Rethinasabapathy, V. Kakani, H. Kim, Y. Park, H.K. Kim, et al., Hexagonal boron nitride composite film based triboelectric nanogenerator for energy harvesting and machine learning assisted handwriting recognition, *Nano Energy* 136 (2025) 110689, <https://doi.org/10.1016/j.nanoen.2025.110689>.
- [21] M.A. García-Rincón, Solar energy materials and Solar cells nanofluids stability in flat-plate solar collectors: a review, *Sol. Energy Mater. Sol. Cells* 271 (2024).
- [22] M. Zhi, S. Yue, L. Zheng, B. Su, J. Fu, Q. Sun, Recent developments in solid-solid phase change materials for thermal energy storage applications, *J. Energy Storage* 89 (2024) 111570, <https://doi.org/10.1016/j.est.2024.111570>.
- [23] Z. Said, A.K. Pandey, A.K. Tiwari, B. Kalidasan, F. Jamil, A.K. Thakur, et al., Nano-enhanced phase change materials: fundamentals and applications, *Prog. Energy Combust. Sci.* 104 (2024) 101162, <https://doi.org/10.1016/j.pecs.2024.101162>.
- [24] O.A. Alawi, H.M. Kamar, A.R. Mallah, S.N. Kazi, NAC. Sidik, Thermal efficiency of a flat-plate solar collector filled with pentaethylene glycol-treated graphene nanoplatelets: an experimental analysis, *Sol. Energy* 191 (2019) 360–370.
- [25] Y. Fu, Y. Xia, X. Lin, Z. Cheng, Z. Zhang, J. Feng, et al., A novel structure design and numerical analysis of porous media-assisted enhanced thermal performance of flat-plate solar collector, *Therm. Sci. Eng. Prog.* 40 (2023), <https://doi.org/10.1016/j.tsep.2023.101777>.
- [26] B. Prabhu, E. Vengadesan, S. Senthil, T. Arunkumar, Comprehensive energy and enviro-economic performance analysis of a flat plate solar water heater with a modified absorber, *Therm. Sci. Eng. Prog.* 54 (2024), <https://doi.org/10.1016/j.tsep.2024.102848>.
- [27] Y. Xia, X. Lin, Y. Shu, Z. Cheng, Enhanced thermal performance of a flat-plate solar collector inserted with porous media: a numerical simulation study, *Therm. Sci. Eng. Prog.* 44 (2023), <https://doi.org/10.1016/j.tsep.2023.102063>.
- [28] T. Sathish, J. Giri, R. Saravanan, M. Ubaidullah, S. Shangdiar, S. Iikela, et al., Amplifying thermal performance of solar flat plate collector by Al203/Cu/MWCNT/SiO2 mono and hybrid nanofluid, *Appl. Therm. Eng.* 252 (2024), <https://doi.org/10.1016/j.applthermaleng.2024.123692>.
- [29] Akram N, Tabatab S, Abdelrazek AH, Khan A, Kazi SN, Sadri R, et al. Solar energy materials and Solar cells application of PEG-Fe 3 O 4 nanofluid in flat-plate solar collector : an experimental investigation 2023;263.
- [30] Anil Kumar, Rajesh Maithani, Masood Ashraf Ali, Naveen Kumar Gupta, Sachin Sharma, Tabish Alam, Hasan Sh Majdi, T.M. Yunus Khan ASY, S.M. Eldin, Enhancement of heat transfer utilizing small height twisted tape flat plate solar heat collector: A numerical study, *Appl. Therm. Eng.* 263 (2024) 1–14, <https://doi.org/10.1016/j.applthermaleng.2023.121844>.
- [31] W. Suqi, Z. Chao, T. Congxiang, Y. Junyi, Use of machine learning in predicting heat transfer and entropy generation in a flat plate solar collector with twisted tape turbulator and ferrofluid under the influence of an external uniform magnetic field: A numerical study, *J. Magn. Magn. Mater.* 590 (2024), <https://doi.org/10.1016/j.jmmm.2023.171657>.
- [32] R. Bharathiraja, T. Ramkumar, M. Selvakumar, K. Sasikumar, Experimental and numerical analysis of hybrid nano-enhanced phase change material (PCM) based flat plate solar collector, *J. Energy Storage* 96 (2024) 112649, <https://doi.org/10.1016/j.est.2024.112649>.
- [33] H.K. Sharma, S. Kumar, S. Kumar, SK. Verma, Performance investigation of flat plate solar collector with nanoparticle enhanced integrated thermal energy storage system, *J. Energy Storage* 55 (2022) 105681, <https://doi.org/10.1016/j.est.2022.105681>.
- [34] B.A.A. Yousef, A. Radwan, A.G. Olabi, M.A. Abdelkareem, Chapter 1.2 - development of solar thermal energy systems, editor, in: A.G. Olabi (Ed.), *Renew. Energy - Vol. 1 Solar, Wind, Hydropower*, Academic Press, 2023, pp. 23–43, <https://doi.org/10.1016/B978-0-323-99568-9.00022-4>.
- [35] Q. Al-Yasiri, M. Szabó, Hourly analysis of temperature and heat gain reduction for building envelope-compacted phase change material in extremely hot conditions, *J. Energy Storage* 68 (2023) 107838, <https://doi.org/10.1016/j.est.2023.107838>.
- [36] M. Alktrane, P. Bencs, Factors affecting nanofluids behaviour: a review, *Int. Rev. Appl. Sci. Eng.* (2023).
- [37] H. Adun, M. Mukhtar, M. Adedeji, T. Agwa, K.H. Ibrahim, O. Bamisile, et al., Synthesis and application of ternary nanofluid for photovoltaic-thermal system: comparative analysis of energy and exergy performance with single and hybrid nanofluids, *Energies* 14 (2021) 4434.
- [38] B.C.C. Pak, Y.I. Cho, Hydrodynamic and heat transfer study of dispersed fluids with submicron metallic oxide particles, *Exp. Heat. Transf.* 11 (1998) 151–170, <https://doi.org/10.1080/08916159808946559>.
- [39] Y. Xuan, W. Roetzel, Conceptions for heat transfer correlation of nanofluids, *Int. J. Heat. Mass Transf.* 43 (2000) 3701–3707, [https://doi.org/10.1016/S0017-9310\(99\)00369-5](https://doi.org/10.1016/S0017-9310(99)00369-5).
- [40] W. Yu, S.U.S. Choi, The role of interfacial layers in the enhanced thermal conductivity of nanofluids: a renovated Maxwell model, *J. Nanoparticle Res.* 5 (2003) 167–171.
- [41] H.C. Brinkman, The viscosity of concentrated suspensions and solutions, *J. Chem. Phys.* 20 (1952) 571.
- [42] S. Alous, M. Kayfeci, A. Uysal, Experimental investigations of using MWCNTs and graphene nanoplatelets water-based nanofluids as coolants in PVT systems, *Appl. Therm. Eng.* 162 (2019) 114265.
- [43] R. Nasrin, N.A. Rahim, H. Fayaz, M. Hasanuzzaman, Water/MWCNT nanofluid based cooling system of PVT: experimental and numerical research, *Renew. Energy* 121 (2018) 286–300, <https://doi.org/10.1016/j.renene.2018.01.014>.
- [44] R.M. Mostafizur, M.G. Rasul, M.N. Nabi, G. Saianand, Properties of Al2O3-MWCNT/radiator coolant hybrid nanofluid for solar energy applications, *Energy Reports* 8 (2022) 582–591, <https://doi.org/10.1016/j.egyr.2022.10.240>.
- [45] I. Umar Ibrahim, M. Sharifpur, J.P. Meyer, Mixed convection heat transfer characteristics of Al2O3 – MWCNT hybrid nanofluid under thermally developing flow: effects of particles percentage weight composition, *Appl. Therm. Eng.* 249 (2024) 123372, <https://doi.org/10.1016/j.applthermaleng.2024.123372>.
- [46] M. Alktrane, Q. Al-Yasiri, K. Saeed Mohammed, H. Al-Lami, P. Bencs, Energy and exergy assessment of a photovoltaic-thermal (PVT) system cooled by single and hybrid nanofluids, *Energy Convers Manag* X 24 (2024), <https://doi.org/10.1016/j.ecmx.2024.100769>.
- [47] M. AbdEl-Rady Abu-Zeid, Y. Elhenawy, M. Bassyouni, T. Majoz, M. Toderas, O. A. Al-Qabandi, et al., Performance enhancement of flat-plate and parabolic trough

solar collector using nanofluid for water heating application, *Results. Eng.* 21 (2024), <https://doi.org/10.1016/j.rineng.2023.101673>.

[48] D. Singh, P. Mall, Experimental investigation of thermal performance of indirect mode solar dryer with phase change material for banana slices, *Energy Sources, Part A Recover. Util Environ. Eff.* (2020) 1–18.

[49] N.S.B. Rukman, A. Fudholi, N.F.M. Razali, M.H. Ruslan, K. Sopian, Energy and exergy analyses of photovoltaic-thermal (PV/T) system with TiO₂/water nanofluid flow, in: IOP Conf. Ser. Earth Environ. Sci. 268, IOP Publishing, 2019 12075.

[50] A.H.A. Al-Waeli, M.T. Chaichan, H.A. Kazem, K. Sopian, J. Safaei, Numerical study on the effect of operating nanofluids of photovoltaic thermal system (PV/T) on the convective heat transfer, *Case Stud. Therm. Eng.* 12 (2018) 405–413.

[51] F. Abbas, H.M. Ali, M. Shaban, M.M. Janjua, T.R. Shah, M.H. Doraneghard, et al., Towards convective heat transfer optimization in aluminum tube automotive radiators: potential assessment of novel Fe₂O₃-TiO₂/water hybrid nanofluid, *J. Taiwan. Inst. Chem. Eng.* 124 (2021) 424–436.

[52] A.M. Hussein, R.A. Bakar, K. Kadrigama, K V Sharma, Experimental measurement of nanofluids thermal properties, *Int. J. Automot. Mech. Eng.* 7 (2013) 850.

[53] Z. Qiu, X. Zhao, P. Li, X. Zhang, S. Ali, J. Tan, Theoretical investigation of the energy performance of a novel MPCM (Microencapsulated Phase Change Material) slurry based PV/T module, *Energy* 87 (2015) 686–698.

[54] M. Firoozzadeh, A.H. Shiravi, M. Lotfi, S. Aidarova, A. Sharipova, Optimum concentration of carbon black aqueous nanofluid as coolant of photovoltaic modules: A case study, *Energy* 225 (2021), <https://doi.org/10.1016/j.energy.2021.120219>.

[55] S.K. Verma, A.K. Tiwari, D.S. Chauhan, Experimental evaluation of flat plate solar collector using nanofluids, *Energy Convers. Manage.* 134 (2017) 103–115, <https://doi.org/10.1016/j.enconman.2016.12.037>.

[56] A. Fudholi, M. Zohri, G.L. Jin, A. Ibrahim, C.H. Yen, M.Y. Othman, et al., Energy and exergy analyses of photovoltaic thermal collector with V-groove, *Sol. Energy* 159 (2018) 742–750.

[57] L.H. Kumar, S.N. Kazi, H.H. Masjuki, M.N.M. Zubir, A. Jahan, C. Bhinitha, Energy, exergy and economic analysis of liquid flat-plate solar collector using green covalent functionalized graphene nanoplatelets, *Appl. Therm. Eng.* 192 (2021) 116916.

[58] A. Farzanehnia, M. Sardarabadi, Exergy in photovoltaic/thermal nanofluid-based collector systems. *Exergy Its Appl. Green Energy Prod. Sustain. Environ.*, IntechOpen, 2019.

[59] M.C. Ndukwu, M.I. Ibeh, P. Etim, C.U. Augustine, I.E. Ekop, A. Leonard, et al., Assessment of eco-thermal sustainability potential of a cluster of low-cost solar dryer designs based on exergetic sustainability indicators and earned carbon credit, *Clean. Energy Syst.* 3 (2022) 100027.

[60] J.J. Michael, S. Iniyar, Performance analysis of a copper sheet laminated photovoltaic thermal collector using copper oxide–water nanofluid, *Sol. Energy* 119 (2015) 439–451.

[61] E. Vengadesan, K. Gnanasekaran, Comprehensive performance analysis of a flat plate solar water heating system featuring a dual-inlet modified absorber, *Discov. Sustain.* 6 (2025) 489, <https://doi.org/10.1007/s43621-025-01361-z>.

[62] KVVC Mouli, L.S. Sundar, A.M. Alklaibi, Z. Said, K V Sharma, V. Punnaiah, et al., Exergy efficiency and entropy analysis of MWCNT/water nanofluid in a thermosyphon flat plate collector, *Sustain. Energy Technol. Assessments* 55 (2023) 102911, <https://doi.org/10.1016/j.seta.2022.102911>.

[63] A.S. Soliman, P. Cheng, 4E analysis of a flat plate solar collector using phase change material and rectangular channels, *Appl. Therm. Eng.* 265 (2025) 125641, <https://doi.org/10.1016/j.applthermaleng.2025.125641>.

[64] S. Rahman, S. Issa, Z. Said, A.A. Hachica, Techno-economic and life cycle analysis of a nano-enhanced flat plate solar collector for improved thermal performance, *Energy Nexus* 18 (2025) 100433, <https://doi.org/10.1016/j.nexus.2025.100433>.

[65] A.K. Sharma, B. Gupta, Performance enhancement of flat plate solar collector system with eutectic form phase change material, *J. Energy Storage* 97 (2024), <https://doi.org/10.1016/j.est.2024.112770>.

[66] R. Bharathiraja, T. Ramkumar, M. Selvakumar, K. Sasikumar, Experimental and numerical analysis of hybrid nano-enhanced phase change material (PCM) based flat plate solar collector, *J. Energy Storage* 96 (2024), <https://doi.org/10.1016/j.est.2024.112649>.

[67] T. Sathish, J. Giri, R. Saravanan, M. Ubaidullah, S. Shangdiar, S. Iikela, et al., Amplifying thermal performance of solar flat plate collector by Al₂O₃/Cu/MWCNT/SiO₂ mono and hybrid nanofluid, *Appl. Therm. Eng.* 252 (2024) 123692, <https://doi.org/10.1016/j.applthermaleng.2024.123692>.

[68] P. Pounraj, D.P. Winston, A.E. Kabeel, B.P. Kumar, A.M. Manokar, R. Sathyamurthy, et al., Experimental investigation on Peltier based hybrid PV/T active solar still for enhancing the overall performance, *Energy Convers. Manage.* 168 (2018) 371–381.

[69] M. Alktranee, M.A. Shehab, Z. Németh, P. Bencs, K. Hernadi, Thermodynamic analysis of mono and hybrid nanofluid effect on the photovoltaic-thermal system performance: A comparative study, *Heliyon* 9 (2023).

[70] B.M. Salim, I.F. Abdulqadir, F.M. Younis, Economic feasibility study of modern and conventional central heating systems for villa located in Duhok City, Iraq, *Eng Technol J* 35 (2017) 725–736.

[71] A.E. Gürel, G. Yıldız, A. Ergün, İ. Ceylan, Exergetic, economic and environmental analysis of temperature controlled solar air heater system, *Clean. Eng. Technol.* 6 (2022) 100369, <https://doi.org/10.1016/j.clet.2021.100369>.

[72] R. Zhu, D. Jing, Numerical study on thermal and melting performances of a horizontal latent heat storage unit with branched tree-like convergent fins, *J. Energy Storage* 62 (2023) 106889, <https://doi.org/10.1016/j.est.2023.106889>.

[73] A.M.A. Alshibil, I. Farkas, P. Víg, Experimental performance comparison of a novel design of bi-fluid photovoltaic-thermal module using Louver fins, *Energy Rep.* 9 (2023) 4518–4531, <https://doi.org/10.1016/j.egyr.2023.03.110>.